Poly(lactic-*co*-glycolic acid) Nanoparticle Delivery of Notch Intracellular Domain Plasmid to Restore Notch Signaling

By

Victoria Messerschmidt

Submitted to the Graduate School of

The University of Texas at Arlington in partial fulfillment

of the requirements for the degree of

Doctor of Philosophy

Department of Bioengineering

University of Texas at Arlington

Research Supervisor: Dr. Juhyun Lee

August 2021

ACKNOWLEDGEMENTS

I would like to thank my family and friends for supporting me through my PhD process. Specifically, I would like to thank my mother for inspiring me to be the best woman I can be, for encouraging me when I needed it, and always having my back. I would also like to thank my dad for supporting me through this journey, first introducing me to scientific papers, and always helping to support me mentally and physically. To my brother and sister, thanks for listening to me and encouraging me to continue to work hard even though I sometimes wanted to quit. I want to also thank Dr. Joe Wolf for always being at my side, talking me through hard times, and making me laugh. Lastly, I want to thank my family for continuing to love me even though I adopted a dog, took in my boyfriend's dog, and then rescued a third.

ABSTRACT

Notch signaling is a highly conserved signaling system that is required for embryonic development and regeneration of organs. When the signal is lost, maldevelopment occurs and leads to a lethal state. Delivering exogenous genetic materials encoding Notch into cells can reestablish downstream signaling and rescue cellular functions. Here, we utilized the negatively charged and FDA approved polymer poly(lactic-co-glycolic acid) to encapsulate Notch Intracellular Domain-containing plasmid in nanoparticles. We show that primary human umbilical vein endothelial cells (HUVECs) readily uptake the nanoparticles with and without specific antibody targets. We demonstrated *in vitro* that our nanoparticles are nontoxic, stable over time, and compatible with blood. We further demonstrated that HUVECs could be successfully transfected with these nanoparticles in static and dynamic environments. We elucidated that these nanoparticles could upregulate the downstream genes of Notch signaling, indicating that the payload was viable and successfully altered the genetic downstream effects. We further tested our optimized nanoparticle *in vivo* using a zebrafish model. We determined that our nanoparticles did not cause severe malformations in the developing embryos, and that they survived development. Additionally, we injected NICD-loaded and anti-Tie2+Tie1 conjugated nanoparticles into 2 days post fertilization zebrafish and show that Notch1b and its related genes are upregulated after 24 hours.

LIST OF FIGURES

FIGURE 2.1: NOTCH SIGNAL ACTIVATION. 13
FIGURE 2.2: CHARACTERIZATION OF PLGA NANOPARTICLES. 28
FIGURE 2.3: RHODAMINE RELEASE FROM HIGH AND LOW MOLECULAR WEIGHT PLGA NPS. 28
FIGURE 2.4: HEMOCOMPATIBILITY OF PLGA NANOPARTICLES. 30
FIGURE 2.5: TARGETING EFFICIENCY OF ANTIBODY CONJUGATED PLGA NANOPARTICLES IN STATIC AND FLOW CULTURE. 32
FIGURE 2.6: STATIC CULTURE OF ANTIBODY CONJUGATED NANOPARTICLES. 33
FIGURE 2.7: ANTIBODY TARGETING SPECIFICITY. 33
FIGURE 2.8: COLONY PCR AND PLASMID VERIFICATION. 34
FIGURE 2.9: CHARACTERIZATION OF GFP-PLGA NPS. 35
FIGURE 2.10: DNA PLASMID LOADED NANOPARTICLES RELEASE CURVES. 36
FIGURE 2.11: GFP PLASMID-LOADED PLGA NANOPARTICLES SUCCESSFULLY TRANSFECT HUVECS 37
FIGURE 2.12: NICD PLASMID-LOADED NANOPARTICLES CAN ENHANCE NICD EXPRESSION IN DYNAMIC CULTURE CONDITIONS 38
FIGURE 2.13: NATURAL UPREGULATION OF NOTCH RELATED GENES FROM SHEAR STRESS. 38
FIGURE 2.14: WESTERN BLOT ANALYSIS OF NANOPARTICLE TREATED HUVECS. 39
FIGURE 3.1: HATCHING AND SURVIVAL RATES FOR EMBRYONIC ZEBRAFISH TOXICITY STUDY. 50
FIGURE 3.2: SURVIVAL OF ZEBRAFISH EMBRYOS. 52
FIGURE 3.3: CHORION DEBRIS FORMATION ON ZEBRAFISH EMBRYOS. 52
FIGURE 3.4: DEVELOPMENTAL DELAYS IN ZEBRAFISH EXPOSED TO VARIOUS CONCENTRATIONS OF PLGA NANOPARTICLES. 52
FIGURE 3.5: PERICARDIAL EDEMA AFTER NANOPARTICLE EXPOSURE. 53
FIGURE 3.6: YOLK SAC EDEMA AFTER PLGA NANOPARTICLE EXPOSURE. 53
FIGURE 3.7: DEVELOPMENT OF BENT TRUNK AFTER NANOPARTICLE EXPOSURE. 53
FIGURE 3.8: TAIL MALFORMATION AFTER NANOPARTICLE EXPOSURE. 54
FIGURE 3.9: COUMARIN-6 LOADED NANOPARTICLES AFTER INJECTION. 54
FIGURE 3.10: COUMARIN-6 NANOPARTICLE TRAVELING IN VESSEL. 55
FIGURE 3.11: COUMARIN-6 NANOPARTICLES ROLLING ON ENDOCARDIUM. 56
FIGURE 3.12: GENETIC EXPRESSION OF NOTCH RELATED GENES AFTER NICD-LOADED ANTI-TIE2+TIE1 CONJUGATED PLGA NANOPARTICLES WERE INJECTED. 57
FIGURE 3.13: CARDIAC MODEL PERFORMANCE. 57
FIGURE 3.14: REPRESENTATIVE IMAGES OF MODEL OUTPUT. 58

List of Tables

Table 2.1: PLGA Nanoparticle Physical Attributes. 27
Table 2.2: Endothelial Cell Targeted PLGA Nanoparticle Attributes. 31
Table 2.3: Plasmid Loaded PLGA Nanoparticle Characteristics. 35
Table 3.1: Cardiac Performance. 59

TABLE OF CONTENTS

COPYRIGHT BY VICTORIA MESSERSCHMIDT II

ACKNOWLEDGEMENTS III

ABSTRACT IV

LIST OF FIGURES V

LIST OF TABLES VI

CHAPTER 1: INTRODUCTION 3

1.1 CARDIAC TRABECULATION BACKGROUND 3
1.2 TRABECULATION DEVELOPMENT IN ZEBRAFISH MODEL 5
1.3 NOTCH SIGNALING 6
1.4 SHEAR STRESS & TRABECULATION 7
1.5 RESCUE OF TRABECULATION AND NOTCH SIGNALING 8

CHAPTER 2: NANOPARTICLE OPTIMIZATION 12

2.1 INTRODUCTION 12
2.2 EXPERIMENTAL SECTION 15
2.2.1 PLGA NANOPARTICLE SYNTHESIS AND CARBODIIMIDE MODIFIED PLGA NANOPARTICLES 15
2.2.2 PLGA NANOPARTICLE CHARACTERIZATION 16
2.2.3 HEMOCOMPATIBILITY OF NANOPARTICLES 18
2.2.4 *IN VITRO* COMPATIBILITY OF NANOPARTICLES 19
2.2.5 DYNAMIC CULTURE SET UP & CELLULAR INTERACTION 21
2.2.6 PLASMID VERIFICATION AND BACTERIA CULTURE 22
2.2.7 PLASMID LOADING INTO OPTIMIZED PLGA NANOPARTICLES 23
2.2.8 PLASMID TRANSFECTION 24
2.2.9 REVERSE TRANSCRIPTASE QUANTITATIVE PCR 24
2.2.10 WESTERN BLOT PROTEIN ANALYSIS 25
2.2.11 STATISTICAL ANALYSIS 26
2.3 RESULTS 26
2.3.1 NANOPARTICLE MOLECULAR WEIGHT OPTIMIZATION 26
2.3.2 HEMOCOMPATIBILITY OF PLGA NANOPARTICLES 29
2.3.3 OPTIMAL ENDOTHELIAL TARGETING ANTIBODY SELECTION 30
2.3.4 PLASMID VERIFICATION 34
2.3.5 PLASMID LOADED PLGA NANOPARTICLE CHARACTERIZATION 34
2.3.6 PLGA NANOPARTICLE TRANSFECTION OVER TIME 36

2.3.7 Effects of Dynamic Culture & Plasmid Loaded Nanoparticles on HUVEC's....37
2.4 Discussion....39
2.5 Conclusions....43

CHAPTER 3: *IN VIVO* NANOPARTICLE ANALYSIS....45

3.1 Introduction....45
3.2 Experimental Section....46
3.2.1 Zebrafish Husbandry....46
3.2.2 Zebrafish Injection....47
3.2.3 *In Vivo* Biodistribution....47
3.2.4 Nanoparticle Dosage & Toxicity Study....47
3.2.5 Reverse Transcriptase Quantitative PCR....48
3.2.6 Cardiac Mechanical Performance....49
3.2.7 Statistical Methods....49
3.3 Results....50
3.3.1 Nanoparticle Dosage & Toxicity Study....50
3.3.2 Biodistribution of PLGA Nanoparticles....54
3.3.3 Reverse Transcriptase Quantitative PCR....56
3.3.4 Cardiac Mechanical Performance....57
3.4 Discussion....59
3.5 Conclusions....61

CHAPTER 4: CONCLUSIONS....62

CHAPTER 5: REFERENCES....64

Chapter 1:

INTRODUCTION

1.1 Cardiac Trabeculation Background

Cardiovascular malformation is the leading cause of birth defects in the developed world [1, 2]. In addition, cardiovascular disease is the number one cause of adult morbidity and mortality in the world [2, 3]. In some of the congenital defects, there are irregular trabeculae that cause many different symptoms. In all mammals, trabeculae exist in both the atrium and the ventricle chambers of the heart. As the embryo grows, the heart begins to contract and mature simultaneously with the embryo maturing. Specifically, the trabeculae are highly organized muscular protrusions in the ventricular lumen that form aft cardiac looping [1, 2]. Trabeculation occurs in a specific pattern across from the atrioventricular (AV) canal in zebrafish [2, 4, 5]. The protrusions radiate from the stereotypical point across from the AV canal and completely cover the ventricle of zebrafish by 5 days post fertilization (dpf) [1, 5, 6]. However, the trabeculae continue to remodel and mature up to 15 dpf [1, 6]. During this time, the cells along the longitudinal axis of the trabeculae are more differentiated on the luminal side of the trabeculae than on the mural side [2]. The trabeculae stop elongating in the luminal direction and become thicker at their bases to become indistinguishable from the compact myocardium [2]. In fact, the trabeculae become the majority of the myocardial mass instead of the compact layer [2, 5]. As the space between the trabeculae decreases, they form vessels, which become the capillaries [2]. The trabeculae continuously remodel with compact layer development, coronary vasculature, and maturation of the conduction system until they are completely mature [2].

In the heart, blood flows directly onto the vessel wall opposite of the heart valve. Transverse flow has been shown to be correlated with atherosclerotic plaque formation in animals by causing endothelial cells to become misaligned [7]. Also, in areas of high stress there is continuous negative remodeling [7]. The heart compensates by increasing the surface area in the form of trabeculae to reduce the stress per area, which could lead to less detrimental effects not seen in the vessels. However, it has been shown that if the blood flow is altered, cardiac abnormalities begin to develop [8].

The primary goal of trabeculation is to make more uniform transmural stress distribution and to increase intramyocardial blood flow [9]. Additionally, myocardial trabeculae have been associated with enhancing contractility [8], ventricular septation [8], and intraventricular conduction [2], and helping to direct blood flow before septation [9]. One group in particular [8] has looked into how changing the biomechanical load on the developing heart effects normal cardiac development. The hemodynamic load was reduced by blocking all of the blood cells from entering circulation, which resulted in the heart volume and myocardial thickness becoming significantly reduced [8]. Acrylamide or TEMED was also placed in the blood vessels to observe the difference between normal hematocrit (TEMED) and slightly reduced hematocrit (acrylamide) on the cardiac development. It was shown that the decrease in hematocrit impairs trabeculation and cardiac looping [8]. Furthermore, circumstances where more oxygen is needed in the cardiac tissue, such as in surgical manipulations or arterial blockages, cause outward or inward remodeling that attempt to return the shear stress back to a healthy physiological range [7].

After observation that trabeculation initiates across the ventricle from a valve [2, 4], Hove *et al*. physically blocked the inlet or outlet to the heart of zebrafish [4]. This caused severe developmental deformations, including the absence of a valve and bulbus [4]. Additionally, cardiac

looping did not occur. Blocking both the inlet and the outlet to the heart caused similar phenotypes, which brought about the conclusion that it is the lack of shear forces in the heart rather than the pressure gradient within the heart that causes these malformations [4].

1.2 Trabeculation Development in Zebrafish Model

There are currently three theories as to how trabeculae start developing: wall buckling from contractions, active invagination of cardiomyocytes into the lumen, active evagination of endocardium into myocardial layer, or a combination of all three [1, 2, 5]. It has been shown that the Neuregulin and *ErbB* pathways regulate ventricular trabeculation in zebrafish [1, 5, 6]. The increase in surface area due to the trabeculae allows for more blood oxygenation and nutrition exchange before coronaries develop [1, 6]. Also, the trabeculae regulate cardiac function by increasing cardiac output [1, 2, 6].

During the development and remodeling phase of trabeculation, a series of events are vulnerable to catastrophic defects. Alterations in cardiogenic events leads to many cardiac diseases like noncompaction cardiomyopathy, diastolic dysfunction, and arrhythmias [2, 10]. Zebrafish are often used in cardiac developmental studies since their gene development and morphogenesis are highly conserved between them and humans [2, 11]. Additionally, zebrafish develop externally, are transparent, and are susceptible to indirect and noninvasive observation of heart development at cellular resolution [2]. It has been shown that hypertrabeculation and hypotrabeculation, an excess and lack of trabeculation, respectively, lead to developmental and functional defects [1, 2, 5, 12, 13]. The reduction in blood flow in *silent heart* (*sih*) or *weak atrium* (*wea*) zebrafish mutants reduces trabeculae, which suggests that proper blood flow is required for maturation of trabeculae [1, 5, 14]. Therefore, the events that occur during trabeculae development are most likely a combination of chemical or genetic signaling and biomechanical force stimulation.

1.3 Notch Signaling

Notch signaling is essential for trabeculation of the heart. The notch ligand is a membrane-bound protein that transmits a signal to the nucleus once activated. This signaling pathway has been shown to be controlled by a manic fringe-dependent manner. Depending on the concentration of the activated fringe family of glycosyltransferases, the selectivity of notch can change between delta-like (DLL) and jagged (Jag) ligands [15]. The manic fringe enzymes alter the selectivity of the notch receptor by elongating the carbohydrates on the extracellular portion of notch. It also regulates the signals that connect the endocardium to the myocardium for trabeculation and chamber development [15]. Therefore, without notch there may not be a way for the endocardium and myocardium to communicate and initiate trabeculation and normal heart development. When the notch ligand is endocytosed, notch physically changes the active sight so that it is able to bind to ADAM metalloproteases. These allow γ-secretase to cleave the ligand to release the notch intracellular domain (NICD) [15]. The NICD then travels to the nucleus and enhances the expression of the target gene.

Endothelial cells are able to sense the magnitude, direction, amplitude, and frequency of fluid flow in their environment [7]. The mechanical forces applied to the cells effect notch signaling. In general, notch signaling in the endocardium is an essential mediator of trabeculation by controlling proliferation and differentiation of trabecular myocytes [16]. Interestingly, when the notch ligand is endocytosed, the mechanical force applied by the bending of the membrane pulls on it and physically changes the active sight so that it can bind to ADAM metalloproteases. This conformational change allows γ-secretase to cleave the ligand and release the NICD [15] so it can travel to the nucleus and bind with recombination signal binding protein for the immunoglobulin k-J region (RBPJ), which is itself bound to notch target genes. While bound to

Notch, RBPJ acts as an activator to enhance the expression of the target gene. When notch is not present, RBPJ acts as a transcriptional repressor [16]. Downstream are two pathways: bone morphogenetic protein-10 (BMP10) in the trabecular myocardium, and ephrine type-B receptor (EPHB-2)-dependent regulation of neuroregulin-1 (NRG1) in the endocardium [16, 17]. Both pathways are extremely important for trabeculae formation.

In brief, it has been shown that exogenous application of BMP10 can effectively rescue chick embryos that are known RBPJ knockouts [16]. These knockouts have an increase in angiogenesis in the myocardium [18] and an increase in cardiomyogenesis in embryonic stem cells when cultured *in vitro* [16]. The RBPJ knockout specifically in the endothelium also has a reduced expression of BMP10, endocardial EPHB2, and NRG1. The increase in cardiomyogenesis results in less trabeculation and therefore shows that notch regulates BMP10 and EPHB1-NRG1 [16].

1.4 Shear Stress & Trabeculation

Lee *et al*. solved the Navier–Stokes' equations that govern the blood flow with a moving wall boundary. With their in-house, stabilized, second-order, finite element method–based flow solver, the group was able to create large-scale simulations of blood flow through zebrafish. Using their computer model, they simulated reduction of shear stress by injecting the *gata1a* MO. This resulted in a reduction of the Average Wall Shear Stress (AWSS) and trabeculation [19]. To ensure that the lack of trabeculation was due to the shear force observed by the cells, the team ran the same simulation but instead changed the blood viscosity to that of the wild-type (WT) zebrafish. This showed that the AWSS between the WT and the adjusted *gata1a* MO zebrafish was the same and therefore supports the shear stress theory [19]. To further prove their hypothesis, the authors used *wea* mutants. This line of mutant zebrafish is unable to contract the atria, which significantly reduces the WSS across from the AV valve. Because of the lack of shear stress, trabeculation does

not form. Injection of the *ErbB2* inhibitor into zebrafish only slightly reduced AWSS compared to *gata1a* MO and *wea* mutants [19]. In an attempt to restore trabeculation, both *gata1a* MO and *NICD* mRNA were injected into the zebrafish and partially restored trabeculation. However, the AWSS remained low in the dual injection fish [19].

Oscillatory fluid flow tends to be concentrated at the trabecular grooves. When pulsatile blood flow is introduced to trabeculae, the force between trabecular ridges creates a vacuum-like force that forces the blood into the cavity. The blood then travels to the bottom of the trabecular groove and up the wall of the first trabecula. Then the blood is forced down again by the pulsatory forces. Altogether, this causes oscillatory flow and therefore OSS between the trabeculae at the trabecular grooves. As the trabeculae continue to mature, the oscillatory shear force increases [19]. If *ErbB2* was inhibited, the nontrabeculated ventricle will have a lower oscillatory force, except for the region of the heart that is across from the atrium inlet [19]. Using the *gata1a* MO and the *wea* zebrafish mutants also caused a lower oscillatory force and resulting OSS at the trabecular bases. However, if *NICD* mRNA was injected as well, the oscillatory force and shear stress were similar to those of WT zebrafish [19].

1.5 Rescue of Trabeculation and Notch Signaling

In chicks, notch can be forcibly expressed using retroviruses. In particular, one group overexpressed the NICD. Interestingly, the chicks had reduced expression of the cardiac myocyte markers [16]. They also showed that overexpression of NICD in endothelial cells induces the Snail family of transcription factors. These then lead to down-regulation of vascular-endothelial (VE)-cadherin and cause morphological changes similar to endothelial-mesenchymal transition (EMT) [16].

A second group used computational modeling from SPIM images in order to determine the effect of the forces of the size of the ventricle in zebrafish. At 75 hpf, those injected with *gata1a* MO were 2.7 ± 0.4 times smaller than the WT control. Similarly, the *tnnt2a* MO group had a 19.0 ± 0.3 times smaller ventricle. When co-injected with *Nrg1* mRNA, the *gata1a* MO group and *tnnt2a* group were only 1.7 ± 0.4 times smaller than the control, where the *tnnt2a* MO + *Nrg1* mRNA zebrafish were similar to the *tnnt2a* MO–only group. At 100 hpf, the ventricles of *gata1a* MO, *tnnt2a* MO, and *gata1a* MO + *Nrg1* mRNA were 1.5 ± 0.4, 23.0 ± 0.3, and 1.0 ± 0.5 times smaller than the WT, respectively [20]. Interestingly, the *Nrg1* mRNA was unable to rescue the *tnnt2a* MO fish (Fig. 8.10B) [20].

Another group, Lee *et al.*, injected *gata1a* MO into zebrafish at the 1–4 cell stage [20]. This MO reduced hematopoiesis by about 90%, which caused a reduction in the shear forces sensed by the cells. After 75 and 100 hpf, there was no trabeculation compared to the WT control [20]. Interestingly, the *gata1a* MO significantly down-regulated notch ligands DLL4, Jag1, and Jag2, receptor Notch1b, and downstream molecules Nrg1 and ErbB2 [20]. This shows that the observed reduction of trabeculation, caused by lowering shear stress, had a direct effect on the cell signaling and specifically in notch-related genes [20]. Using *Tg(flk:mCherry, tp1:gfp)* zebrafish to visualize the notch signaling specifically in the heart, they showed that the *gata1a* MO significantly reduced the shear stress in the endocardium [20]. Similarly, they used the *wea* zebrafish mutant, where atrial contraction cannot occur. The absence of atrial contraction does not produce the shear stress that usually occurs across from the AV canal. In these zebrafish, the ventricle was small and there was also no trabeculation. Additionally, the notch signaling ligands, receptor, and downstream molecules were all down-regulated [20].

In hopes of restoring trabeculation, Lee *et al*. injected *Nrg1* mRNA into the zebrafish at the embryonic stage. In both the *wea* mutant and the *gata1a* MO zebrafish, the *Nrg1* mRNA up-regulated the notch signaling–related genes at 75 and 100 hpf [20]. In addition to the up-regulated notch genes, the *wea* mutant also had enhanced cardiac contraction and ventricular function [20].

The *tnnt2a* MO was also used to stop myocardial contraction. The lack of contraction would lead to a lack of cardiac strain and shear stress, which was thought to prevent trabeculation. The *tnnt2a* MO led to a significant down-regulation of the notch signaling molecules and genes. At 100 hpf, the ventricle of the *tnnt2a* MO zebrafish was thin and did not have trabeculation (Fig. 8.11K) [20].

The *clo* zebrafish mutant develops without the endocardium, which would essentially determine whether it is the endocardium or the myocardium that senses biomechanical forces. When cultured, the *clo* mutant had significant down-regulation of notch signaling, and at 100 hpf, the ventricular wall was very thin and had no trabeculation (Fig. 8.11L) [20]. Additionally, the *clo* mutant had little cardiac mRNA for notch ligands, receptor, and target genes [20]. To support the theory that it is the endothelium that senses the forces and not the lack of endothelium that causes the lack of trabeculation in the *clo* mutant, human aortic endothelial cells (HAECs) were subjected to PSS. At a force of 23 dyne cm^{-2} and a rate of 1 Hz, the PSS up-regulated notch-related genes. Additionally, when notch signaling was inhibited, the notch expression returned to normal [20]. In these experiments, it is shown that the endocardium senses the shear stress caused by blood flow. Interestingly, the addition of *EPO* mRNA, which codes for blood cells, did not change the development of the trabeculae, even with the increase in viscosity. Also, the regulation of Notch genes was similar to that of the control [20]. Treating the zebrafish embryos with isoproterenol to increase the contractility, and therefore the shear force, did not have a significant effect on the

trabecular network or notch signaling expression [20]. The increase in heart rate could be related to athletes. Those who participate in intense cardio-exercise increase their heart rate and therefore increase the shear force on the endocardium. It could be that the added shear stress is what makes exercise beneficial to heart health.

Chapter 2:

NANOPARTICLE OPTIMIZATION

2.1 Introduction

Notch signaling is highly conserved cell signaling pathway, which is involved in diverse embryonic organs or tissue development as well as regeneration [15, 16, 21-28]. Notch signaling regulates cell-fate determination during activation by signal sending and receiving, affected through ligand-receptor crosstalk. During the cell-fate decisions in cardiac [1, 2, 26], neuronal [29-31], immune [32, 33] and endocrine [34, 35] development, the Notch signaling pathway acts as a key regulator of cell proliferation and differentiation [15, 36, 37]. Notch receptors are single-pass transmembrane proteins composed of functional Notch extracellular domain (NECD), transmembrane (TM), and Notch intracellular domains (NICD). Notch receptors are processed in the endoplasmic reticulum and Golgi apparatus within the signal-receiving cell, through cleavage and glycosylation, generating a Ca^{2+}-stabilized heterodimer composed of NECD non-covalently attached to the transmembrane NICD inserted in the membrane called S1 cleavage.

Regulation of arteriovenous specification and differentiation in both endothelial cells and vascular smooth muscle cells are also involved in Notch signaling including regulation of blood vessel sprouting, branching during normal and pathological angiogenesis, and the physiological responses of vascular smooth muscle cells [15, 16, 18, 25, 38, 39]. Defects in Notch signaling also cause inherited cardiovascular diseases, such as Left Ventricular Noncompaction and Alagille syndrome [15, 16, 38]. In endothelium, Delta-like ligand 4 (DLL4) is one of main ligands to send a signal to Notch in the adjacent cell [15, 25] (**Figure 2.1A**). This in turn signals the surrounding cells to determine the cell-fate [15]. Once Notch is activated, the NICD is cleaved by γ-secretase

and translocated into the nucleus (**Figure 2.1B-C)**. Here, the NICD binds directly to the DNA, physically moving corepressors and histones, recruiting coactivators, and activating gene transcription (**Figure 2.1D**) [15, 25, 37].

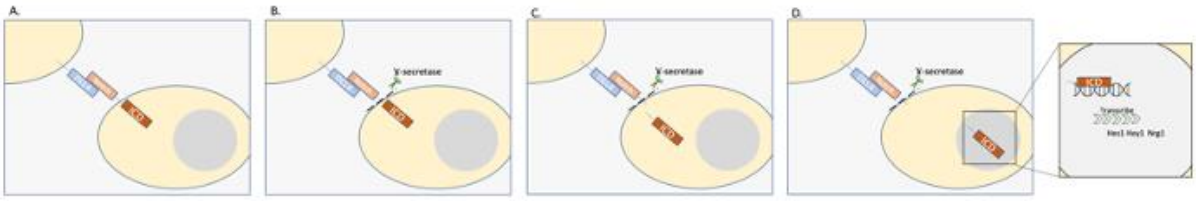

Figure 2.1: Notch Signal Activation. *(A) Notch Receptor and DLL4 ligand bind together. (B) γ-secretase cleaves the Intracellular domain (ICD) from the extracellular domain. (C-D) The ICD is released and travels into the nuclease. (D inset) The ICD binds onto the DNA as a transcription factor to transcribe downstream Notch genes such as Hes1, Hey1 and Nrg1.*

When a disruption in this Notch pathway occurs, either by chemical or genetic means, it causes developmental malformations. For example, significant reduction of Notch signaling causing cardiac trabeculation is usually associated with deficient compaction in the ventricle [20, 25]. It has been shown that lack of cardiac trabeculation results in the inability to dissipate the kinetic energy, resulting in a malformed heart due to a decrease in Notch related signaling [19, 20]. Interestingly, when given NICD mRNA injection treatment, the heart function – including end diastolic function, end systolic function, stroke volume, and ejection fraction – were all partially or fully restored by rescuing downstream Notch signaling [19, 40]. Regardless of whether the defect comes from the γ-secretase's inability to cleave the NICD, or if the native NICD is defective and unable to pass through the nucleus, by providing NICD mRNA to the cell it partially rescued the trabeculation. Similarly, when Notch signaling is inhibited from NICD cleavage or NICD translocation into the nucleus, Notch related downstream genes can rescue the feedback loop of Notch pathway[20]. These data demonstrate the possible impact of spatiotemporal NICD treatment for therapeutic approach to rescue Notch signaling.

Traditionally, retroviruses or liposomes have been used to deliver cDNA plasmids [22, 41-43]. These methods have various benefits such as DNA protection and DNA viability, but also have limitations of nonspecific delivery, stability after formulation, or host immune responses [44, 45]. Therefore, many groups are attempting to deliver the genetic materials such as cDNA plasmids via nanoparticles to mitigate these negative effects. Various polymers have been used for gene delivery [46-51]. Cationic polymers have been used extensively to deliver genetic materials, as DNA condenses quickly on the oppositely charged positive polymer. These polymers can be synthetic or organic and usually include polyethylenimine [52, 53], polyamidoamine [54, 55], chitosan [56, 57], and cationic proteins [58] or peptides. However, the drawbacks of these highly positively charged polymers are mainly due to its toxicity [44, 45] and often require extensive surface modifications to alleviate those effects [45]. Poly(lactic-co-glycolic acid) (PLGA), an FDA-approved biodegradable polymer [59], is a negatively charged polymer that has been extensively used for cancer treatment [60-63]. More recently, PLGA has been used to load both hydrophilic and hydrophobic materials such as cDNA plasmids [47] and RNAs [64], proteins [65-67], dyes [68], and drugs [69].

In this study, we developed the PLGA nanoparticles encapsulating plasmids containing NICD for upregulation of Notch pathway molecules in cultured HUVECs. Using a flow chamber mimicking the *in vivo* circulation system, we evaluated the toxicity, stability, and compatibility in blood of the PLGA nanoparticles and our data suggested that we have here demonstrated NICD cDNA plasmid in the PLGA nanoparticles could upregulate Notch pathway molecules.

2.2 Experimental Section

2.2.1 PLGA Nanoparticle Synthesis and Carbodiimide modified PLGA Nanoparticles

Poly(D, L-lactide-*co*-glycolic acid) nanoparticles (PLGA, 50:50, Akina Inc., West Lafayette, IN, USA) of two different molecular weights including 55–65 kDa (High Molecular Weight (HMW) Nanoparticles) and 5–10 kDa (Low Molecular Weight (LMW) Nanoparticles) were fabricated by a standard double emulsion method as previously described [50]. In brief, PLGA was dissolved in chloroform (Sigma-Aldrich, St. Luis, MO, USA) at a 20 $mg \cdot mL^{-1}$ concentration. Following which, the water phase with 1% (w/w) rhodamine B (Rh B) was added to the oil phase dropwise under stirring and sonicated. The primary emulsion is then emulsified into 5% (w/v) Poly(vinyl) Alcohol (PVA, 13 kDa, Sigma-Aldrich) solution and then sonicated at 40 Watts for 5 minutes (30 sec off every 1 minute). Nanoparticles were then collected via centrifugation at 15,000 RPM for 15 minutes, then lyophilized until completely dry. Coumarin-6 loaded PLGA nanoparticles were prepared to track the nanoparticles' interaction with the cells. For this, coumarin-6 was added into the oil phase at a ratio of 1:100 with respect to the amount of PLGA used during the nanoparticle synthesis. Rh B loaded nanoparticles were exclusively used to study model drug release kinetics.

PLGA nanoparticles were conjugated either with anti-EGFL7 antibody (ab92939, Abcam) or anti-Tie2+Tie1 antibody (ab151704, Abcam) via EDC-NHS chemistry as described elsewhere with modification [50]. In brief, nanoparticles were suspended in 0.1M MES buffer at a concentration of 2 mg/ml. Following which, 120 mg of EDC and 150 mg of NHS was added into the solution. After 2 hours of incubation at room temperature, nanoparticles were collected by centrifugation and resuspended in PBS (2mg/ml). 25µL of antibody solution was added into nanoparticles solution and incubated overnight at 4^{o}C. The supernatant was used to determine the

antibody conjugation efficiency using Bradford assay following manufacturers' instructions. Pellets were resuspended in DI water, freeze-dried, and stored for use.

2.2.2 PLGA Nanoparticle Characterization

2.2.2.1 Dynamic Light Scattering & Zeta Potential

To determine the size and surface charge, nanoparticle suspension was added to a transparent cuvette and was then inserted into the ZetaPALS dynamic light scattering (DLS) detector (NanoBrook 90Plus PALS, Brookhaven Instruments, Holtsville, NY) as previously described [50]. Scanning electron microscopy (SEM, Hitachi S-3000N, Hitachi, Pleasanton, CA) was used to visualize the morphology of nanoparticles. Briefly, 50 µl of the nanoparticle suspension air-dried on a coverslip was silver sputter-coated and inserted into the SEM instrument. To determine the *in vitro* stability, nanoparticles were suspended in saline (0.9% Sodium Chloride, NaCl, Crystalline, Fisher Scientific, Hampton, NH, USA) or Vasculife VEGF basal cell media with 10% Fetal Bovine Serum (LL-0003, Lifeline Cell Technologies) and incubated at 37ºC for 48 hours. Particle size was measured on predetermined time points using DLS as described earlier. The stability of the nanoparticles was represented as the percentage change of nanoparticle size measured at each time point with respect to initial particle size according to the following equation:

$$Size\ (\%) = \frac{Nanoparticle\ Size_{t=t_0}}{Nanoparticle\ Size_{t=0}} * 100 \qquad \text{(Equation 1)}$$

2.2.2.2 Nanoparticle Stability

To determine the size and surface charge, nanoparticle suspension was added to a transparent cuvette and was then inserted into the ZetaPALS dynamic light scattering (DLS) detector (NanoBrook 90Plus PALS, Brookhaven Instruments, Holtsville, NY) as previously described [50]. Scanning electron microscopy (SEM, Hitachi S-3000N, Hitachi, Pleasanton, CA)

was used to visualize the morphology of nanoparticles. Briefly, 50 µl of the nanoparticle suspension air-dried on a coverslip was silver sputter-coated and inserted into the SEM instrument. To determine the *in vitro* stability, nanoparticles were suspended in saline (0.9% Sodium Chloride, NaCl, Crystalline, Fisher Scientific, Hampton, NH, USA) or Vasculife VEGF basal cell media with 10% Fetal Bovine Serum (LL-0003, Lifeline Cell Technologies) and incubated at 37ºC for 48 hours. Particle size was measured on predetermined time points using DLS as described earlier. The stability of the nanoparticles was represented as the percentage change of nanoparticle size measured at each time point with respect to initial particle size according to the following equation:

$$Size\ (\%) = \frac{Nanoparticle\ Size_{t=t_0}}{Nanoparticle\ Size_{t=0}} * 100 \qquad \text{(Equation 2)}$$

2.2.2.3 Drug Release Kinetics

Low and high molecular weight nanoparticles were loaded with rhodamine B using a double emulsion method. Nanoparticles at either low or high molecular weight particles were suspended in 1X PBS (1 mg·mL^{-1}, n=3) and placed into dialysis bags to only allow Rhodamine B passage. The samples were placed in 50 mL tubes and filled with 20 mL of 1X PBS and incubated at 37°C. At each time point, 1 mL of the solvent was removed and stored at -20°C and replaced with 1 mL of fresh 1X PBS. Each sample had their absorbance read, and had the amount released calculated using a standard curve.

The encapsulation efficiency of entrapped reagent including, pCAG-GFP or TetO-FUW-NICD, within PLGA nanoparticles was determined based on indirect loading analysis. Briefly, the un-loaded reagent in the supernatant (PVA solution) following the nanoparticle synthesis, was used to calculate the encapsulation efficiency (Equation 2). The amount of plasmid was determined using Picogreen DNA assay (#E2670, Promega, Madison, WI) following the manufacturers' instructions.

$$Encapsulation\ Efficiency\ (\%) = \frac{Plasmid\ initially\ added - plamid\ in\ supernatant}{Plasmid\ initially\ added} * 100 \qquad \text{(Equation 2)}$$

For *in vitro* plasmid release studies, solutions of pCAG-GFP or TetO-FUW-NICD plasmid-loaded nanoparticles were prepared in 1X PBS at a concentration of 1.5 mg/mL. At predetermined time points, the samples were centrifuged at 12,000 RPM for 5 minutes. The supernatant was then collected and stored at -20ºC for further analysis. Pellet was again resuspended in fresh 1mL of PBS solution and incubated until next time point. Four replicates were used for analysis. For analysis, the plasmid solutions were incubated with Nb.Bsmi nicking enzyme (R0706S, New England Biolabs) for 60 minutes at 65ºC in NEBuffer 3.1. The enzyme was then inactivated for 20 minutes at 80ºC. The nicked plasmid supernatant was analyzed for plasmid release using the Picogreen DNA assays. The plasmid standards were made to determine the cumulative percentage of plasmid release over time.

2.2.3 Hemocompatibility of Nanoparticles

HMW nanoparticles and LMW nanoparticles compatibility was evaluated using human whole blood, to determine hemolysis and whole blood clotting kinetics assay as previously mentioned. For these studies, whole blood was drawn from healthy adult volunteers into acid citrate dextrose anticoagulant tubes (ACD, Solution A; BD Franklin Lakes, NJ). Consent from the volunteers was obtained prior to the blood collection, and all the procedures strictly adhered to the IRB standards approved at the University of Texas at Arlington.

For whole blood clotting, human blood was diluted 1:10 using saline (0.9% NaCl). Following which, 50 µL of activated blood was added into 10 µL of saline diluted nanoparticle solution at concentration of 1 $mg{\cdot}mL^{-1}$. The samples were then exposed to ambient air for 0, 10, 20, 30, and 60 minutes at n = 6. At each time point, 1.5 mL of DI water was added to lyse the un-

clotted blood. The top 200 μL of solution was transferred to a 96-well plate and the absorbance was read at 545 nm. Saline diluted blood with no treatment served as a control.

In the hemolysis study, high molecular weight and low molecular weight unloaded nanoparticles were suspended in saline at the following concentrations (0, 10, 25, 50, 100, 250, 500, 1000 $\mu g \cdot mL^{-1}$). Human blood was diluted with DI water 1:50 for the positive control. The negative control was human blood diluted 1:50 with saline. The samples were incubated with 200 μL of saline-diluted blood for 2 hours at 37°C. Following the incubation, the samples were centrifuged at 1,000 g for 10 minutes. The top 100 μL of each sample was placed in a 96-well plate and had its absorbance read at 545 nm. The percent hemolysis was calculated using the following equation:

$$\% = \frac{Abs_{sample} - Abs_{neg\ ctl}}{Abs_{pos\ ctl} - Abs_{neg\ ctl}} \times 100$$

2.2.4 *In vitro* Compatibility of Nanoparticles

HUVECs were cultured in M199 media (M4530, Sigma-Aldrich) supplemented with Vasculife VEGF LifeFactors kit (LS-1020, Lifeline Cell Technologies) up to passage 7 in a 5% CO_2 environment. To determine the compatibility of nanoparticles, HUVECs were seeded in 96 well plates at seeding density of 8,000 cells/well and cultured overnight. Coumarin-6 loaded HMW- and LMW-PLGA nanoparticles of various concentrations (25, 50, 100, 250, 500, 1000 μg mL^{-1}) were prepared in complete M199 media and added to the cells. After 24 hours of incubation at 37°C, the nanoparticle containing media was removed, and cells were carefully washed with 1X PBS. The cellular viability was then determined using MTS assays per manufacturer's instructions.

To determine the uptake of coumarin-6 loaded HMW- and LMW-PLGA nanoparticles by HUVECs, cells were seeded in 96 well plates at a density of 8,000 cells/well. After overnight

culture, nanoparticles of various concentrations 50, 100, 250, 500, 1000 $\mu g \cdot mL^{-1}$ were added to the cells and incubated for 4 hours in 37°C. Nanoparticles were then removed, cells were carefully washed with PBS solution and lysed using 1% Triton X-100. Fluorescence intensity measurement of nanoparticles in cellular lysate was quantified at a wavelength of 457 nm (excitation)/500 nm (emission) using a spectrophotometer. These measurements were analyzed against a nanoparticle standard. The measurements were further normalized with respect to the sample cellular protein amount as determined based on BCA assay (Thermofisher Scientific).

Similarly, interaction between antibody (anti-EGFL7 or anti-Tie2+Tie1) conjugated HMW nanoparticles loaded with coumarin-6 and HUVECs were also determined under static conditions. In brief, nanoparticle suspensions were treated with cells for 1 hour and following which, cells were washed and lysed. Cellular lysate was used to determine the amount of nanoparticle attachment and internalization with HUVECs based on coumarin-6 fluorescence intensity. These fluorescence measurements values were then normalized with the total DNA content per sample using Picogreen DNA assays per manufacturer's instructions. In parallel, nanoparticle interaction with HUVECs were observed using a fluorescence microscope under FITC channel. The cells were counterstained using Nucblue (Invitrogen) to visualize the cell nuclei.

To show the specificity of the optimal antibody to endothelial cells, HL-1 cells were cultured overnight in a 96-well plate overnight in Claycomb media supplemented with 10% FBS, 1% pen-strep, 0.1 mM Norepinephrine, and 2 mM of L-Glutamine. The following day, nanoparticles conjugated with anti-Tie2+Tie1 were added to the HL1 cells at 100, 250, 500, 1000 $\mu g \cdot mL^{-1}$ for 4 hours. After the incubation, cells were lysed, and fluorescence read under the same conditions. The fluorescence was normalized to DNA content.

In addition, the ability of a coumarin-6 loaded, antibody (anti-EGFL7 or anti-Tie2+Tie1) conjugated HMW nanoparticles to adhere and interact with HUVECs under physiological relevant flow condition was investigated. HUVEC's were seeded at $2*10^6$ cells/mL into μSlide $VI^{0.4}$ channel and cultured overnight. Following the cell attachment, nanoparticles suspended in M199 media at a concentration of 200 μg/mL were perfused through the channels of the flow slide using Ibidi pump system at a shear stress of 5 dyne/cm^2 for 30 minutes. Later, cells within the channels were fixed with paraformaldehyde solution and treated with Nucblue (Invitrogen) to stain cell nuclei. The cellular images were then taken using fluorescence microscope under FITC and DAPI channel to visualize the nanoparticles and nuclei, respectively. The fluorescence intensity of nanoparticles was later quantified using NIH ImageJ software and normalized by cell number.

To further prove our nanoparticle selectivity, we coated μ-Slide IV 0.4 (Ibidi, #80606) with 14.4 μg of bovine serum albumin (BSA), a 1:1 solution of Tie1 and Tie2 protein at 14.4 μg, or 1X PBS. The solutions were left at room temperature for 2 hours. The remaining solution was washed off with 1x PBS. Coumarin-6 nanoparticles were prepared as above, and conjugated with either BSA, anti-Tie2+Tie1, or were unconjugated. Nanoparticle media at a concentration of 250 μg/mL was flowed through at 5 dyne·cm^{-2} for 15 minutes. The media was removed and washed with 1X PBS to remove unbound nanoparticles. The slides were imaged at 100x to visualize the bound content. Using ImageJ, the intensity of the fluorescence was measured to quantitatively evaluate the binding.

2.2.5 Dynamic Culture Set Up & Cellular Interaction

Viscosity of cell culture media was measured using the Discovery Hybrid Rheometer (HR-2, Waters TA Instruments). Specifically, M199 media completed with Vasculife VEGF Endothelial Medium (Lifeline Cell Technology, LL-0003) and up to 10% FBS, and 4% w/v Dextran (MW

2×10^6, Sigma) in M199 media with 10% FBS was measured. Using an orbital shaker (Cole Parmer, EW-51900-19), the revolutions per minute were calculated using the following equation:

$$\tau_{max} = a\sqrt{\eta\rho(2\pi f)^3}$$

Where τ is the shear stress (dyne·cm^{-2}), a is the orbital radius of the shaker (cm), ρ is the density of the culture media (g·mL^{-1}), η is the viscosity of the media measured (poise), and f is the frequency of rotation (rotations·sec^{-1})[70-73]. The shear stresses calculated were 5 and 12 dyne·cm^{-2}.

HUVECs were seeded in M199 media and cultured overnight, or until 75% confluent. The following day, the cells were placed on the orbital shaker and set to a rotation speed to equal 5 or 12 dyne·cm^{-2}. After 24 hours of orbital shaking, the experimental groups were added at a concentration of 250 μg·mL^{-1}. The groups added were empty PLGA Nanoparticles, NICD-loaded nanoparticles, NICD-loaded nanoparticles with conjugated anti-Tie2+Tie1. No treatment was added as a control. The cells were then placed back on the orbital shaker for another 24 hours. The cells were used for either RT-PCR analysis, or western blotting.

2.2.6 Plasmid Verification and Bacteria Culture

TetO-FUW-NICD was a gift from Rudolf Jaenisch (Addgene plasmid #61540) and pCAG-GFP was a gift from Connie Cepko (Addgene plasmid #11150). Plasmid stabs were obtained and streaked across LB agar plates with ampicillin antibiotic. The plates were cultured for 24 to 48 hours at 37°C for colony formation. Eleven colonies were picked and cultured in liquid LB broth with ampicillin antibiotic at 37°C and 100-200 RPM overnight.

After overnight culture in LB broth, bacteria were pelleted via centrifugation at 3,000 RPM for 20 minutes. The supernatant was removed, and the pellet stored in -20°C or used for

isolation. To isolate the plasmid, the Qiagen Plasmid *Plus* Mega Kit was used following the manufacturer's instructions. Elutants were quantified using a nanodrop and stored in -20°C until needed. To ensure that the bacteria was positively transfected with TetO-FUW-NICD, colony PCR was conducted. Primers were used to amplify the insert are as follows: NICD (Frd CGGCGGCAGCATGGCCAGC, Rev CTTGAACGCCTCCGGGATGCGG), GFP (Frd ATGTTCATGCCTTCTTCTTTTTCCTACAGC, Rev ATGATGTCCCCATAATTTTTGGCAGAGGG). Colonies with positive transfection were stored in 25-50% glycerol in -80°C for future use. To verify the TetO-FUW-NICD plasmid, 1 μg of plasmid was digested with 20 units of NdeI enzyme in 10x CutSmart Buffer and nuclease free water for a 50 μL reaction volume. The reaction was incubated at 37°C for 15 minutes, then at 65°C for 20 minutes to inactivate NdeI. The digest was then run on a 1% agarose gel with a 1kb Ladder for reference. pCAG-GFP was digested with EcoRI and NotI for 15 minutes in 10X NEBuffer 3.1 and nuclease free water (to 50 μL) at 37°C. Then, it was heated to 65°C for 20 minutes to inactivate the enzymes. The digest was run on a 1% agarose gel with a 1 kb Ladder for quantification. The sequences were run to ensure that there was no recombination of the plasmid during the bacteria culture.

2.2.7 Plasmid Loading into Optimized PLGA Nanoparticles

pCAG-GFP or TetO-FUW-NICD loaded HMW nanoparticles were also prepared based on the same standard double emulsion method with slight modifications according to past literature[74]. In brief, 250 μg of plasmid was diluted in 5% glucose solution to 200 μL which was then emulsified into 0.5 mL of 5% (w/v) PLGA solution in chloroform using a probe sonicator at 40W energy output for 15s to form primary water/oil emulsion. The primary emulsion was then emulsified into 3 mL of 4% (w/v) PVA solution by sonication and later dropped into 7.5 mL of

0.3% (w/v) PVA solution while stirring. The final mixture was then stirred for 3 hours at room temperature and particles were collected by centrifugation. Nanoparticles were then lyophilized until completely dry before use.

2.2.8 Plasmid Transfection

HUVECs were seeded 24 hours prior to the transfection study at n=4. The following day, Lipofectamine 3000 or no treatment were applied to the cells for 6 hours. After the treatment, the cells were washed three times with 1X PBS and incubated until the next time point. HMW PLGA nanoparticles were prepared as described above. The nanoparticles at a concentration of 250 μg/mL were then applied to HUVECs for 6 hours. The cells were then gently washed with 1X PBS three times and new media given. The cells treated with Lipofectamine, nanoparticles, or no treatment were then grown for 24, 48, or 72 hours post transfection. Cells transfected with pCAG-GFP plasmid-loaded nanoparticles were imaged in a fluorescent microscope on FITC channel, nuclei were stained with Nucblu. The intensity of each fluorescent channel was measured via ImageJ. The data was then normalized by cell number, via Nucblu intensity, then normalized to the untreated cell group following the Equation 4.

$$Mean\ Correlated\ Total\ Cell\ Fluorescence = (GFP\ Intensity) / (NucBlu\ Intensity) \quad \text{(Equation 4)}$$

Before loaded into nanoparticles, the quality and quantity of TetO-FUW-NICD plasmid were analyzed by digestion to ensure positive clones were used. Four biological repeats were carried out for each experiment.

2.2.9 Reverse Transcriptase Quantitative PCR

Cells were first washed with 1X PBS two to three times. Then, 0.025% trypsin was added for 5 minutes at 37ºC to allow cell detachment. The trypsin was then neutralized by adding media

twice the volume of trypsin to the wells. The cells were collected, centrifuged at 150×g for 5 minutes, and the supernatant discarded. The cells were then used to isolate the total RNA using the Aurum Total RNA Mini Kit (Biorad, #7326820) following the manufacturer's instructions. RNA concentration was determined via NanoDrop, by reading each sample 3 times. The total RNA was then used to synthesize 200 ng of cDNA using the iScript Synthesis Kit (Biorad, #1708890) following the manufacturer's instructions. PCR was conducted using the iTaq Universal SYBR Green Supermix (Biorad, #1725121) following manufacturer's instructions. The primer sequences for human mRNA are as follows: *Dll4* (Frd CTGCGAGAAGAAAGTGGACAGG, Rev ACAGTCGCTGACGTGGAGTTCA), *Hes1* (Frd GGAAATGACAGTGAAGCACCTCC, GAAGCGGGTCACCTCGTTCATG*)*, *Hey1* (Frd ACCATCGAGGTGGAGAAGGA, Rev AAAAGCACTGGGTACCAGCC), *Notch1* Receptor (Frd GGTGAACTGCTCTGAGGAGATC, Rev GGATTGCAGTCGTCCACGTTGA), NICD (Frd ACCAATACAACCCTCTGCGG, Rev GGCCCTGGTAGCTCATCATC), and *β-Actin* (CGACAGGATGCAGAAGGAG, Rev ACATCTGCTGGAAGGTGGA).

2.2.10 Western Blot Protein Analysis

HUVEC's were cultured in a 6-well plate overnight. The following day, nanoparticles loaded with NICD plasmid, nanoparticles loaded with NICD plasmid and conjugated anti-Tie2+Tie1, blank nanoparticles, or cell media were added to the culture. After an additional 24 hours with treatment and shear stress of 12 dyne·cm^{-2}, the media was removed, cells washed with 1x PBS, and lysed with radioimmunoprecipitation assay buffer supplemented with protease inhibitor cocktail (Roche). Protein concentrations were determined via the Pierce BCA Assay Kit (ThermoFisher). Antibodies against Notch1 (Invitrogen, MA5-32080), Hey1 (Abnova, H00023462-M02), and Hes1 (OriGene, TA400013), were probed at suggested dilutions.

Secondary antibodies conjugated with horseradish peroxidase were incubated and detected by enhanced chemiluminescence reagent (BioRad). The total protein of each well was measured using ImageJ's Gel Analysis. Similarly, each individual band was measured using the same technique, then normalized to the total protein amount.

2.2.11 Statistical Analysis

All statistics were evaluated in the statistical program R. For the percent change in size, a one-way ANOVA was used to compare each sample to its' original size. A one-way ANOVA was also used to determine significance of nanoparticle uptake between anti-Tie2+Tie1 or anti-EGFL7 nanoparticles, antibody uptake in dynamic culture, nanoparticle dose study, and gene expression between static and dynamic culture. A two-sample t-test was used to compare the HMW to LMW in the cell viability and nanoparticle cellular interaction studies. Similarly, the gene expression was evaluated to compare dynamic culture at 12 dyne·cm^{-2} to static culture for each gene. All values where $p < 0.05$ were considered significant. Post-hoc Tukey tests were conducted if ANOVA results showed significance to determine differences between groups.

2.3 Results

2.3.1 Nanoparticle Molecular Weight Optimization

Before performing the cell study, nanoparticles were characterized based on their size, poly dispersity, and zeta potential (**Table 2.1**). The diameter of high molecular weight (HMW) PLGA nanoparticles, at 55–65 kDa, were smaller than the low molecular weight (LMW), 1–5 kDa, PLGA nanoparticles at 234 ± 90 and 246 ± 85 nm, respectively. The zeta potential, or surface charge of the nanoparticles, indicates the presence of the negatively charged carboxyl and hydroxyl groups

present on the polymer. The HMW PLGA nanoparticles have a charge of -31 ± 3.4 mV, and the LMW PLGA nanoparticles have a charge of -29 ± 2.8 mV. The poly dispersity of both the HMW and LMW PLGA nanoparticles, 0.13 ± 0.05 and 0.08 ± 0.02 respectively, shows that the particles are uniformly dispersed. SEM images also indicated that both the HMW- and LMW-nanoparticles were uniformly dispersed and have spherical morphology (**Figure 2.2A**).

Table 2.1: PLGA Nanoparticle Physical Attributes.

PLGA Nanoparticles	Size (nm)	Poly Dispersity	Zeta Potential (mV)
Molecular Weight: 1 – 5 kDa	234 ± 90	0.13 ± 0.05	-31 ± 3.4
Molecular Weight: 55 – 65 kDa	246 ± 85	0.08 ± 0.02	-29 ± 2.8

Following *in vitro* stability studies using HMW- and LMW-nanoparticles in both saline (0.9% NaCl) and 10% serum, the nanoparticle percent size change was determined. Accordingly, the diameter of HMW nanoparticles were constant in both formulations over 48 hours of incubation, which indicates the superior stability properties of HMW nanoparticles. On other hand, the size of LMW nanoparticles steadily increased over time and showed significant aggregation following their incubation with the saline solution at 24 hours. In serum, the LMW nanoparticles increased in size, but was not significantly different (**Figure 2.2B**). This suggests that LMW nanoparticles were not stable and may exhibit aggregation behavior following their suspension and/or administration. Then, the drug release kinetics were then compared between the two molecular weights using a model hydrophilic drug Rh B. High and low molecular weight nanoparticles were incubated in 1X PBS over a period to assess Rh B release kinetics. Both molecular weights of PLGA nanoparticles showed a burst release of Rh B dye with LMW releasing all the dye within 5 days and the HMW nanoparticles with a sustained release of over 20% by day 28 (**Figure 2.3**).

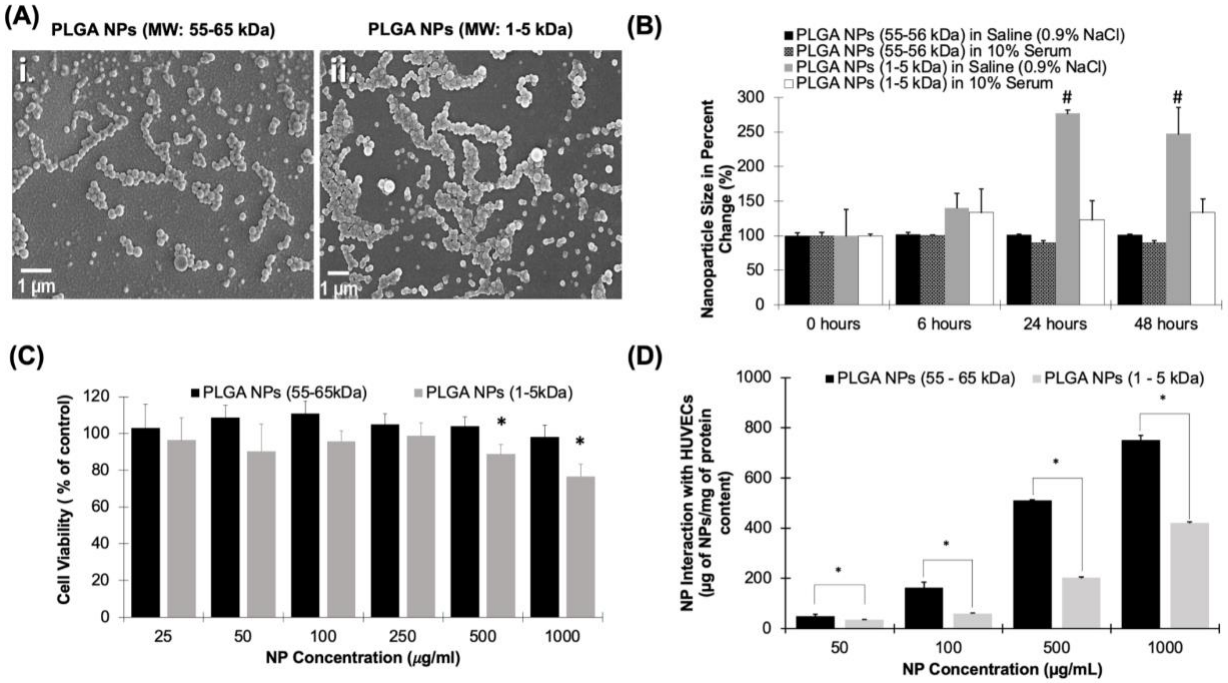

Figure 2.2: Characterization of PLGA Nanoparticles. *(A) SEM images of (i) PLGA at 55 – 65 kDa and (ii) PLGA at 1– 5 kDa nanoparticles. Scale bar is 1 um. (B) Nanoparticles stability in saline (0.9% NaCl) or 10% Serum over time shows that the HMW PLGA nanoparticles' size is steady in both solutions, while the LMW PLGA nanoparticles vary in both the Saline and 10% Serum. Error bars denote standard error. (C) Cytocompatibility test comparing HMW to LMW PLGA nanoparticles. This shows that HMW PLGA Nanoparticles do not affect the cell viability at all tested concentrations. At high concentrations, the LMW PLGA Nanoparticles cause cell toxicity, which results in cell death. (D) HUVEC uptake of both HMW and LMW PLGA nanoparticles shows HMW had significantly higher uptake than LMW at all concentrations. Data shown as mean +/- standard error. ($p < 0.05$).*

To assess the cytocompatibility of nanoparticles, HUVECs were subjected to varying concentrations of both HMW and LMW nanoparticles. Across all tested concentrations, the HMW nanoparticles were all above 90% viability, while the LMW had greater than 90% viability in only 25, 50, 100, and 250 µg/mL **(Figure 2.2C)**. At both 500 and 1,000 µg/mL, the LMW nanoparticles were

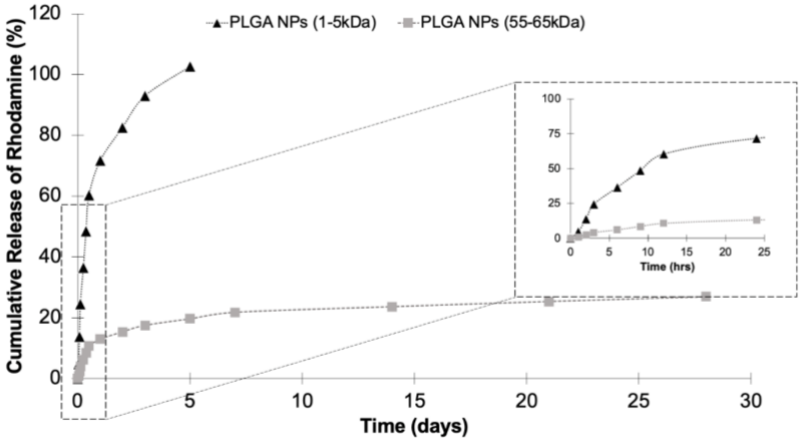

Figure 2.3: Rhodamine release from High and Low Molecular Weight PLGA NPs. *Rhodamine Release in High and Low Molecular Weight PLGA. Release of Rhodamine into the supernatant has a burst release, followed by a sustained release up to 28 Days. The Low Molecular Weight nanoparticles release 100% of loaded rhodamine by 5 days. Inset shows initial burst release up to 24 hours.*

significantly lower at 88 ± 10% and 76 ± 13% viability, respectively ($p < 0.05$). The uptake of the nanoparticles was evaluated using HUVECs incubated with varying amounts of nanoparticles. At each tested concentration, the HMW nanoparticles had a significantly higher uptake compared to that of the LMW. Additionally, there is a trend showing a dose-dependent relationship between the number of nanoparticles applied, and the number of nanoparticles endocytosed by the cells (**Figure 2.2D**).

2.3.2 Hemocompatibility of PLGA Nanoparticles

To simulate the effect of nanoparticles on human blood, hemolysis and whole blood clotting tests were conducted. For whole blood clotting, the nanoparticles significantly affected the clotting cascade only during the first 10 minutes of exposure. Afterwards, the progress of blood clotting gradually reduced and there were no significant results compared to whole blood without exposing PLGA nanoparticles (**Figure 2.4A**). After 60 minutes, blood exposed to either HMW or LMW nanoparticles had great low supernatant absorbance, 0.1, similar to whole blood which indicates blood clot. Our results reflect those who have performed similar studies showing little red blood cell lysis or reduced clotting kinetics [75]. Furthermore, the interaction between red blood cells and nanoparticles were evaluated by incubation with diluted blood to determine if hemolysis occurred. Compared to lysed cells as the positive control, both the HMW and LMW nanoparticles were significantly lower (< 0.25%) in hemolysis **(Figure 2.4B).**

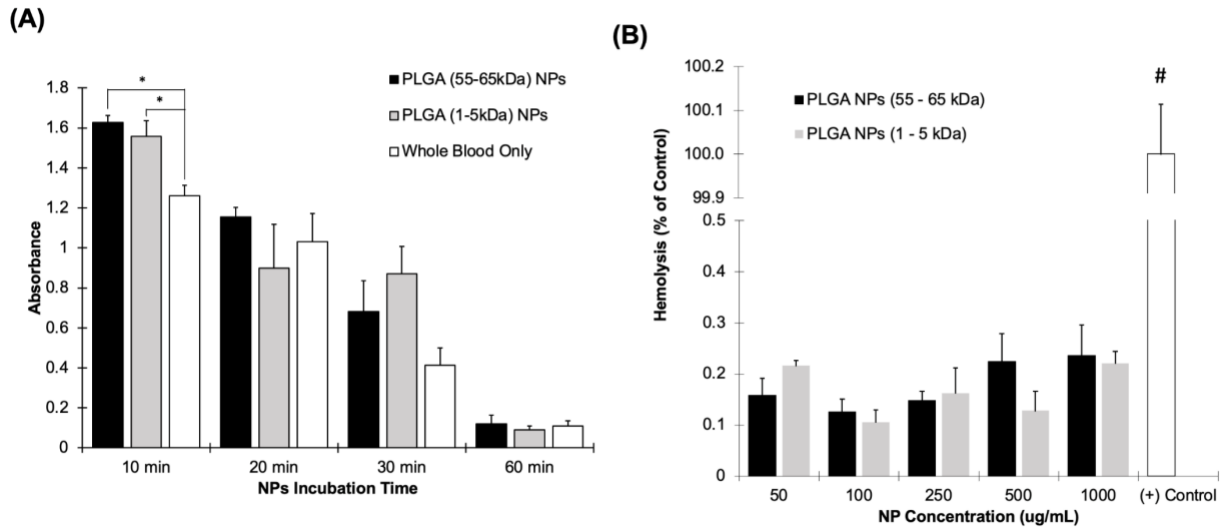

Figure 2.4: Hemocompatibility of PLGA Nanoparticles. *(A) Nanoparticles at a concentration of 1 mg/mL were subjected to human blood for up to 1 hour. The clotting was significantly affected only during the first 10 minutes of nanoparticle exposure ($p < 0.05$). At all other time points, the nanoparticles did not affect the clotting ability of the human blood. Blood exposed to only air was kept as a control. * denoted a significant difference with $p < 0.05$ (B) Nanoparticles were incubated with blood for 1 hour. Compared to RO water treatment (Positive control), both nanoparticle groups had significantly less hemolysis at all tested concentrations. # indicates that the Positive control is significantly higher than all other groups with $p < 0.05$. All data is shown as mean + standard error.*

2.3.3 Optimal Endothelial Targeting Antibody Selection

For this study, HMW nanoparticles were used because the HMW has greater cell uptake and cell viability properties even though LMW nanoparticles have a rapid release profile. Anti-EGFL7 and Anti-Tie2+1 were conjugated to PLGA HMW nanoparticles and characterized. The nanoparticles conjugated with anti-EGFL7 increased to 249 ± 55 nm, while the nanoparticles conjugated with anti-Tie2+Tie1 are 243 ± 41 nm. Both antibody conjugations had a low poly dispersity, indicating that most of the nanoparticles were uniform in size. The antibodies changed the surface charge of the nanoparticles from -31 ± 3.4 to -23.5 ± 1.7 mV for anti-EGFL7 nanoparticles, and -31 ± 3.4 to -27.4 ± 1.8 mV for anti-Tie2+Tie1 nanoparticles. The antibodies had a conjugation efficiency of 59.6 ± 1.5% and 47.5 ± 1.2% for anti-EGFL7 conjugated nanoparticles and anti-Tie2+Tie1 conjugated nanoparticles, respectively (**Table 2.2**).

Table 2.2: Endothelial Cell Targeted PLGA Nanoparticle Attributes.

Antibody Conjugated Nanoparticles	Size (nm)	Poly Dispersity	Zeta Potential (mV)	Conjugation Efficiency (%)
Anti-EGFL7 PLGA NPs	249 ± 55	0.21 ± 0.01	-23.5 ± 1.7	59.6 ± 1.5
Anti-Tie2+Tie1 PLGA NPs	243 ± 41	0.19 ± 0.13	-27.4 ± 1.8	47.5 ± 1.2

Furthermore, we tested our antibody conjugated particles on their uptake abilities under static and physiological flow conditions. Under static conditions, we saw concentration-dependent uptake of nanoparticles by endothelial cells (**Figure 2.5A**). As the concentration of anti-Tie2+Tie1 conjugated nanoparticles increases, the rate of cellular uptake increases 3.5-folds and 8.4 folds from 100 μg/mL to 250 and 500 μg/mL, respectively (**Figure 2.5A)**. Similarly, anti-EGFL7 conjugated nanoparticles increase 2.4-folds and 5.1-folds from 100 μg/mL to 250 and 500 μg/mL, respectively. Yet, the unconjugated nanoparticles increase 5.2-folds and 7.3-fold from concentrations of 100 to 250, and 500 μg/mL, respectively. Additionally, antibody conjugated nanoparticles had a greater interaction with the cells compared to unconjugated ones. Coumarin-6 loaded HMW nanoparticles conjugated to either anti-EGFL7 or anti-Tie2+Tie1 supported the quantitative data (**Figure 2.6**).

Compared to unconjugated nanoparticles, antibody conjugated nanoparticles to target endothelial cells show higher uptake efficiency although the diameter of nanoparticles were increased **(Figure 2.5B).** Tested with flow system, nanoparticles conjugated with anti-EGFL7 has significantly higher cellular uptake. However, nanoparticles conjugated with anti-Tie2+Tie1 were significantly higher in cellular uptake than that of anti-EGFL7 conjugated. With fluorescent imaging, we can visualize that under flow conditions at 12 dyne·cm^{-2}, the antibody conjugated nanoparticles were able to be endocytosed into cells at a higher rate compared to unconjugated

nanoparticles **(Figure 2.5C)**. To further prove the targeting ability of our anti-Tie2+Tie1 nanoparticles, we tested their binding ability to different protein coatings. In addition to anti-Tie2+Tie1 coated nanoparticles, we compared BSA conjugated and unconjugated nanoparticles on their binding ability to Tie1+Tie2-coated, BSA-coated, or uncoated slides. The Tie2+Tie1 nanoparticles bound to the Tie2+Tie1-coated slides significantly higher than both the BSA conjugated nanoparticles and the unconjugated nanoparticles **(Figures 2.7A-B)**. Additionally, we cultured cardiomyocytes, HL1 cells, with anti-Tie2+Tie1 nanoparticles to investigate if the NP uptake was specific to endothelial cells. There was a significant difference at all tested concentrations between HUVECs and HL1 cells **(Figure 2.7C)**.

Due to the increase in cellular uptake of nanoparticles conjugated with anti-Tie2+Tie1, this antibody was determined to be superior for endothelial targeting.

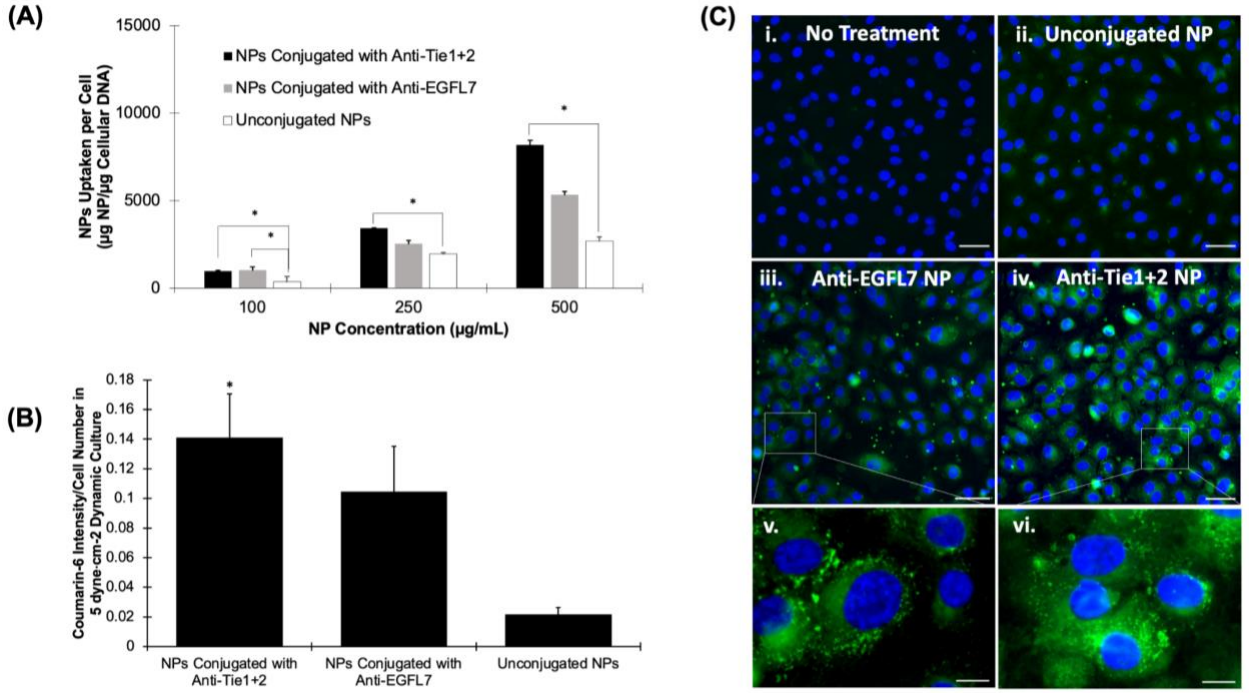

Figure 2.5: Targeting Efficiency of Antibody Conjugated PLGA Nanoparticles in Static and Flow Culture. *(A) HUVEC Cellular uptake of endothelium specific anti-EGFL7, anti-Tie1+2 conjugated nanoparticles or unconjugated nanoparticles after 4 hours. (B) HUVEC Cellular uptake under 5 dyne·cm^{-2} of endothelium specific anti-EGFL7 and anti-Tie1+2 conjugated nanoparticles, or unconjugated nanoparticles. (C) Fluorescent images of HUVEC's incubated in flow culture of dyne·cm^{-2} with (i) No Treatment, (ii)*

Unconjugated Nanoparticles, (iii) Anti-EGFL7 conjugated nanoparticles, (iv) anti-Tie1+2 conjugated nanoparticles. Scale bar = 20 μm. Zoomed in portions of HUVEC's incubated in flow culture at dyne·cm^{-2} with (v) Anti-EGFL7 conjugated nanoparticles, and (vi) anti-Tie2+Tie1 conjugated nanoparticles. Scale bar = 5 μm.

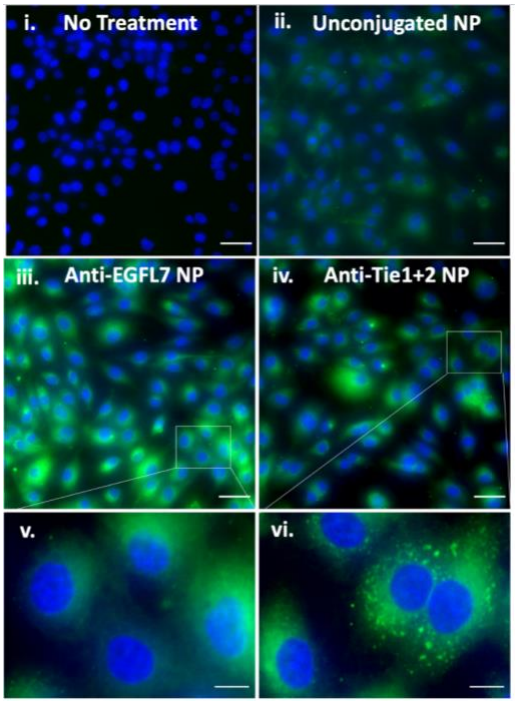

Figure 2.6: Static culture of antibody conjugated nanoparticles. *HUVEC's cultured with media only (i.), unconjugated nanoparticles (ii.), anti-EGFL7 conjugated nanoparticles (iii.), or anti-Tie2+Tie1 conjugated nanoparticles (iv.). Scale bar = 20 um. Higher magnification of HUVEC's cultured in anti-EGFL7 conjugated nanoparticles (v.) or anti-Tie2+Tie1 conjugated nanoparticles. Scale bar = 5 um.*

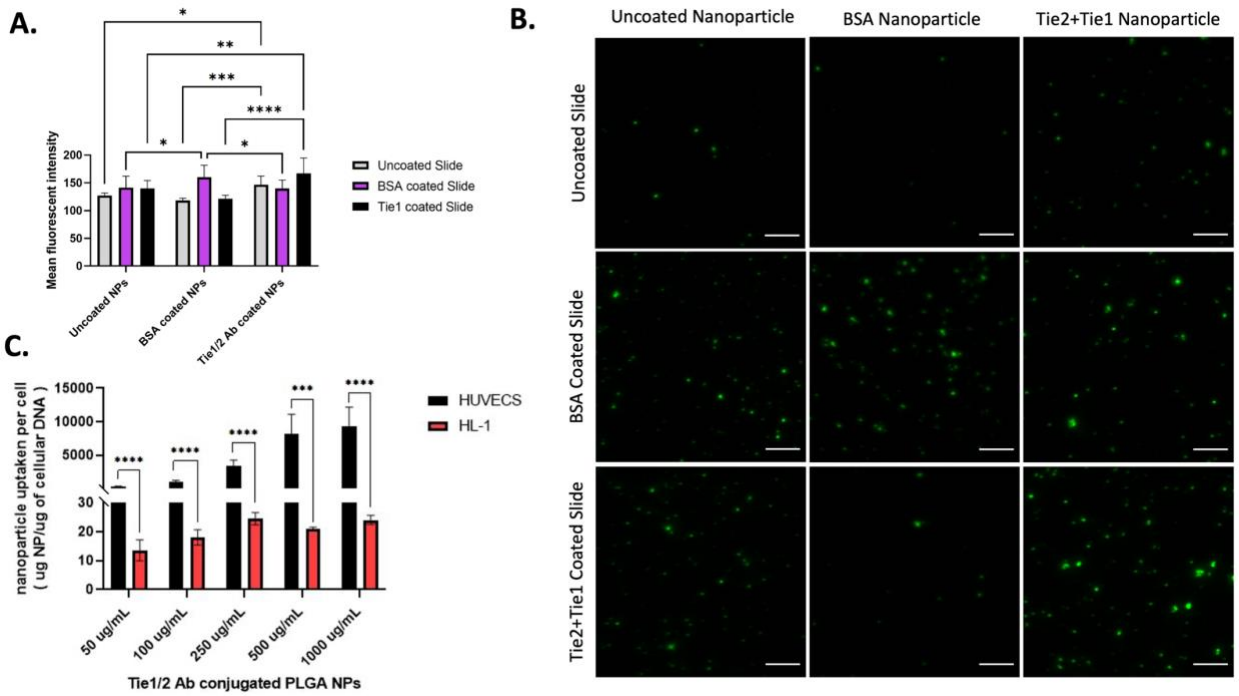

Figure 2.7: Antibody Targeting Specificity. *(A) Quantitative evaluation of protein coated nanoparticles (BSA, Tie2+Tie1, or uncoated NPs) flowed over protein coated slides (BSA, Tie2+Tie1, or uncoated slides) at 5 dyne/cm^2. * indicates ($p < 0.05$), ***

*indicates (p < 0.01), *** indicates (p < 0.001), **** indicates (p < 0.0001) evaluated using a two-way ANOVA.(B) Qualitative images of coumarin-6 nanoparticles with differing protein coatings. Scale bar = 5 μm. (C) Cellular uptake analysis of anti-Tie2+Tie1 conjugated nanoparticles cultured with HUVECs and HL1 cells. *** indicates (p < 0.001), **** indicates (p < 0.0001) evaluated via t-test per concentration. All data shown as mean + standard deviation.*

2.3.4 Plasmid Verification

After TetO-FUW-NICD bacteria was cultured overnight, the plasmid was isolated and stored. After expansion and digestion, the digestion product was run on a 1% gel and showed that 10 out of 11 colonies were positive for the TetO-FUW-NICD plasmid (**Figure 2.8A**). Both the pCAG-GFP and TetO-FUW-NICD plasmids were digested to ensure gene accuracy. The pCAG-GFP plasmid was digested with EcoRI and NotI enzymes for 15 minutes at 37°C. The enzymes cut the GFP plasmid to make two bands at 772 bp and 4,790 bp (**Figure 2.8B**). Similarly, the TetO-FUW-NICD plasmid was cut with the dual cutter NdeI making bands at 3,409 bp and 7,262 bp (**Figure 2.8C**). Lastly, the plasmids were verified using LNCS primers (results not shown here).

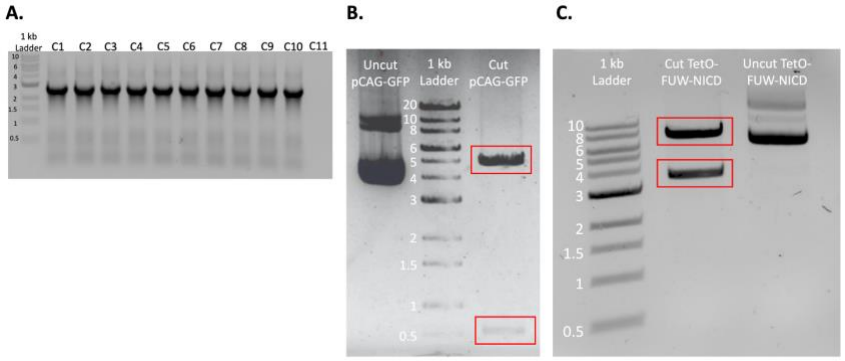

Figure 2.8: Colony PCR and Plasmid Verification. *(A) Colony PCR showing that after expansion, there was no recombination during bacteria culture. (B) pCAG-GFP plasmid before and after being digested with EcoRI and NotI. (C) TetO-FUW-NICD plasmid before and after being digested with NdeI.*

2.3.5 Plasmid Loaded PLGA Nanoparticle Characterization

Both pCAG-GFP and TetO-FUW-NICD were loaded into HMW PLGA nanoparticles at 62.3 ± 2.2 μg plasmid per mg of nanoparticles and 89.1 ± 6.4 μg plasmid/mg nanoparticles, respectively. The encapsulation efficiency of 56.3 ± 4.1% and 38.9 ± 2.17% for NICD and GFP

plasmids, respectfully, is similar to previous reports [76-78] (**Table 2.3**). Additionally, previously reported particles were larger [77] and the encapsulated plasmids were 6- to 2-times smaller in size [76-78] of our largest plasmid, at 10,671 bp, the genetic material encapsulated into the nanoparticles was released in a similar form to our model hydrophilic drug, Rh B (**Figure 2.10A, 2.3, 2.9**). The NICD plasmid released up to 1 μg of plasmid within the first 24 hours. The plasmid continued to be released over 14 days to a total of 1.2 μg (**Figure 2.10A**). Our GFP plasmid loaded nanoparticles similarly released 0.5 μg of plasmid over 14 days (**Figure 2.9**). With the addition of the plasmids, the zeta potential and size both increased, indicating a change. However, the polydispersity value was still low illustrating their homogeneous size.

Table 2.3: Plasmid Loaded PLGA Nanoparticle Characteristics.

	Size (nm)	Poly Dispersity	Zeta Potential (mV)	Encapsulation Efficiency (%)
NICD Plasmid Loaded	272 ± 51	0.119 ± 0.05	-12.87 ± 1.895	56.3 ± 4.1%
NICD Plasmid Loaded Nanoparticle with Anti-Tie2+Tie1	268 ± 26	0.107 ± 0.01	-17.03 ± 0.827	

TetO-FUW-NICD loaded nanoparticles were also given to HUVECs at varying doses. Compared to the untreated group, Notch target gene, *Hey1* was upregulated in each tested concentration. Additionally, another target gene, *Hes1*, was upregulated with NICD plasmid concentrations of 100, 250 and 500 μg of nanoparticles while 1000 μg of NICD plasmid loaded nanoparticle decrease the expression level

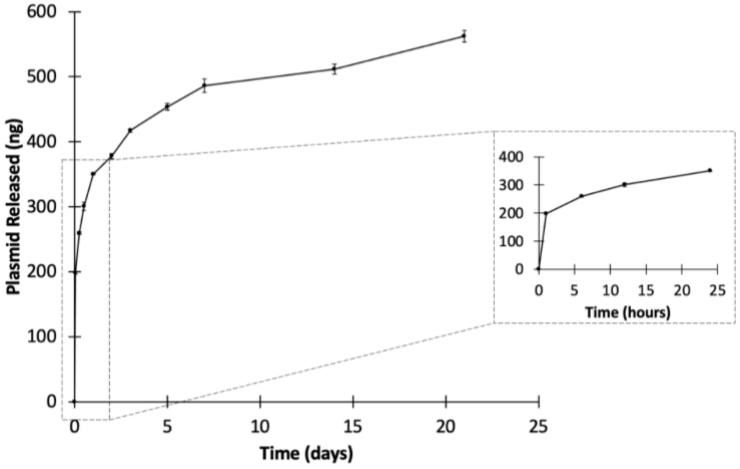

Figure 2.9: Characterization of GFP-PLGA NPs. *(A) GFP plasmid released from HMW PLGA nanoparticles over 21 days.*

of *Hey1* (**Figure 2.10B**). Based on the trend, the NICD plasmid concentration of nanoparticle, affects the gradual expression level of target gene expressions until adding 250 ug of NICD plasmid loaded NP.

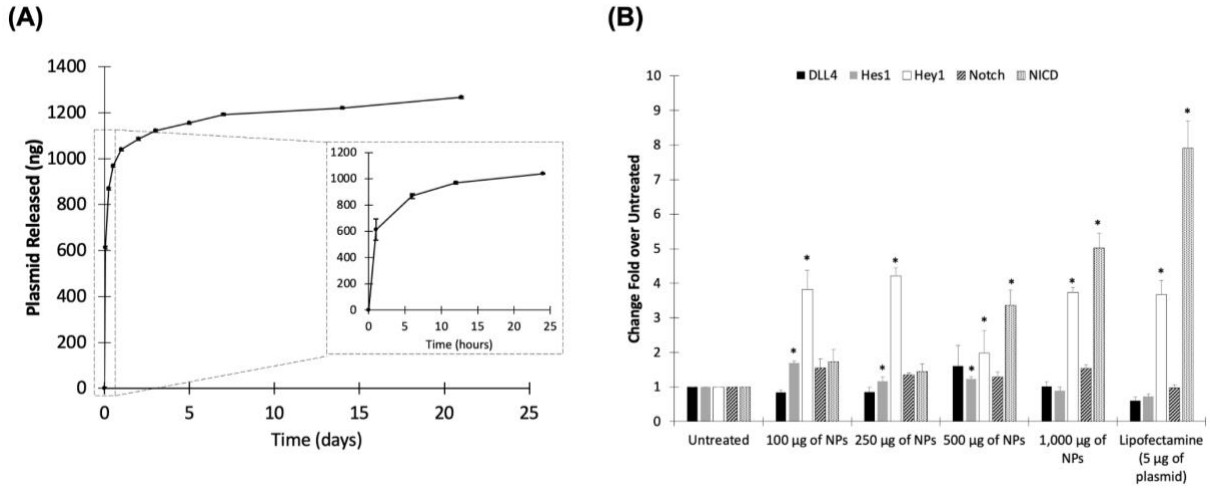

Figure 2.10: DNA Plasmid loaded nanoparticles Release Curves*. Release curve of (A) NICD Plasmid-loaded nanoparticles measured via Promega dsDNA assay after 21 days. n = 3. Data shown as mean +/- standard deviation. (B) Quantitative expression of NICD after TetO-FUW-NICD Nanoparticle transfection at varying dosages. *significantly different from Untreated Group.*

2.3.6 PLGA Nanoparticle Transfection over Time

HUVECs were subjected to 5 µg of plasmid, either through Lipofectamine 3000, or our GFP Plasmid-loaded nanoparticles. After 6 hours, the treatments were removed, and fresh media applied to the cells. At 12 hours, there were not many cells that expressed GFP. At 24 hours, the lipofectamine group had much higher cell death than that of the GFP Plasmid nanoparticle group. Additionally, the GFP plasmid-loaded nanoparticles had an even expression of GFP across most cells. At 24 hours, the lipofectamine group had few GFP positive cells compared to that of the nanoparticle treated group. At 48 hours post transfection, GFP was observed in both lipofectamine treated and GFP plasmid-loaded nanoparticle treated groups. The lipofectamine had a brighter GFP signal at 48 hours compared to the nanoparticle treatment, however, the nanoparticles transfected a higher number of cells, which lead the 5 µg of plasmid to be more evenly spread

among cells (**Figure 2.11A)**. The GFP plasmid-loaded nanoparticle group had a higher survival rate and high transfection efficiency.

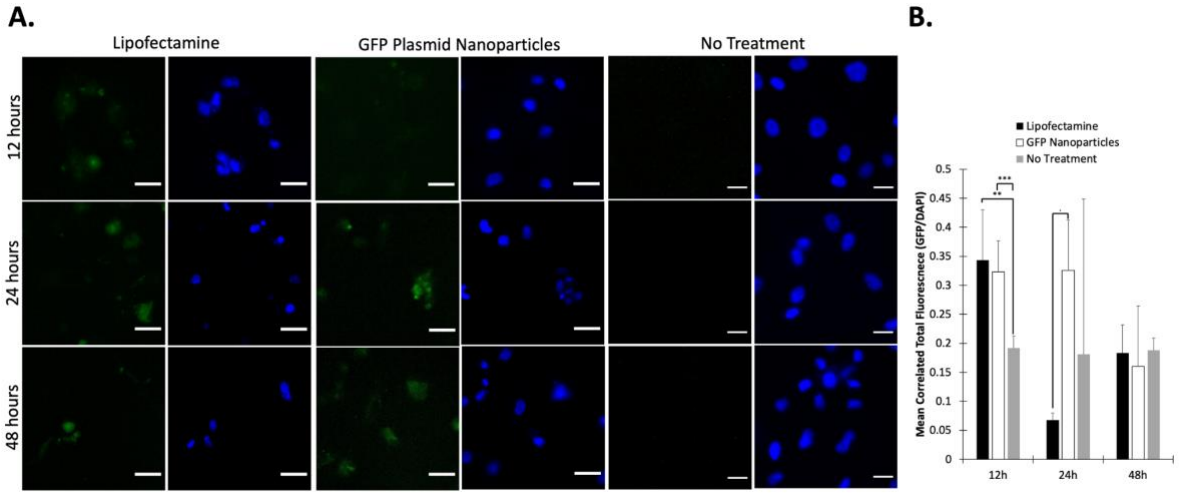

Figure 2.11: GFP plasmid-loaded PLGA nanoparticles successfully transfect HUVECs*. (A) After 6 hours of treatment, nanoparticles or lipofectamine were washed off with 1X PBS and media replaced. At 12 hours, slight GFP expression can be seen (A, first row). After 24 hours, there is significantly more GFP expression in GFP plasmid-loaded nanoparticles than lipofectamine treated cells (A, second row). Additionally, after 48 hours, lipofectamine transfected cells had a high GFP signal in few cells. Whereas nanoparticle transfected cells had many cells expressing GFP, resulting in a lower over signal. (B) Normalized GFP intensity to nuclei intensity shows significantly higher lipofectamine at 12h, significantly higher Nanoparticle at 24h, and no difference at 48h. · indicates ($p < 0.1$), ** indicates ($p < 0.01$) and *** indicates significance at ($p < 0.001$) via one-way ANOVA per time point.*

2.3.7 Effects of Dynamic Culture & Plasmid Loaded Nanoparticles on HUVEC's

HUVECs were subjected to 12 dyne·cm^{-2} for 24 hours, then an additional 24 hours of flow treatment with blank nanoparticles, TetO-FUW-NICD loaded HMW nanoparticles, TetO-FUW-NICD loaded HMW nanoparticles conjugated with anti-Tie2+Tie1, or cell media only for control. Each nanoparticle group was given at a concentration of 250 μg/mL due to highest Notch target efficiency concentration **(Figure 2.12)**. The plasmid-loaded nanoparticles with targeting antibody had significantly higher expression of Notch related genes, but not *Hes1* although expression level was upregulated **(Figure 2.12)**. The expression of Notch related genes when exposed to plasmid-loaded nanoparticles without a conjugating antibody were not significantly different from that of the blank nanoparticles. Both were upregulated most likely due to the increased viscosity of the media after adding the nanoparticles. The higher viscosity causes a higher shear stress, which

upregulates shear responsive Notch signaling **(Figure 2.13A)**. In addition, the shear stress induces the HUVECs to align with the direction of the flow **(Figure 2.14B)**. We then analyzed the protein expression after application of the NICD loaded nanoparticles, NICD loaded nanoparticles conjugated with anti-Tie2+Tie1, blank nanoparticles, or no treatment. After 24 hours of treatment, we found that the nanoparticles containing NICD plasmid had a significantly higher amount of Hey1, NICD, and Hes1 proteins compared to the cells only group **(Figure 2.14)**.

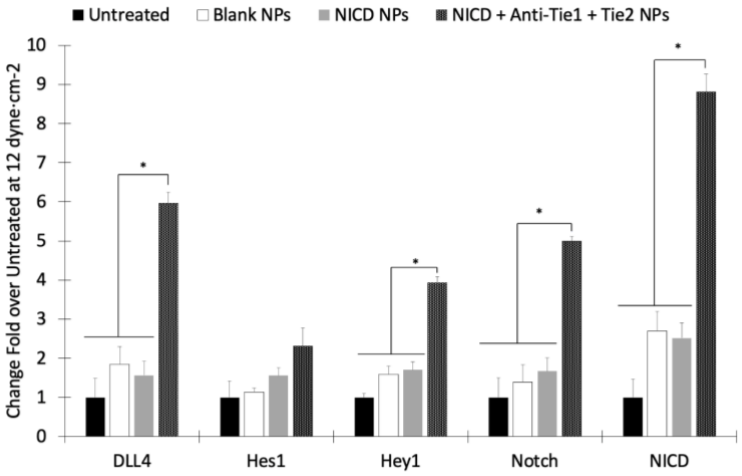

Figure 2.12: NICD Plasmid-loaded Nanoparticles can Enhance NICD Expression in Dynamic Culture Conditions*. RT-PCR results showing that NPs conjugated to anti-Tie2+Tie1 significantly upregulate DLL4, Hey1, Notch Receptor and NICD in 12 dyne/cm^2 flow conditions. * NICD+Anti-Tie1+Tie2 is significantly higher ($p < 0.05$).*

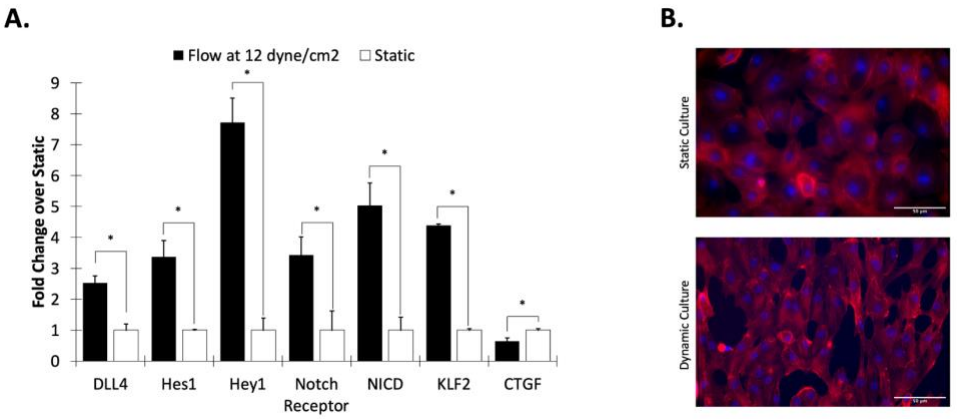

Figure 2.13: Natural upregulation of Notch related genes from shear stress. *(A) RT-PCR results showing that notch related genes are upregulated from shear stress stimulus. (B) HUVECs cultured under 12 dyne·cm^{-2} of shear stress for 24 hours. Flow direction is horizontal. Scale bar = 50 μm.*

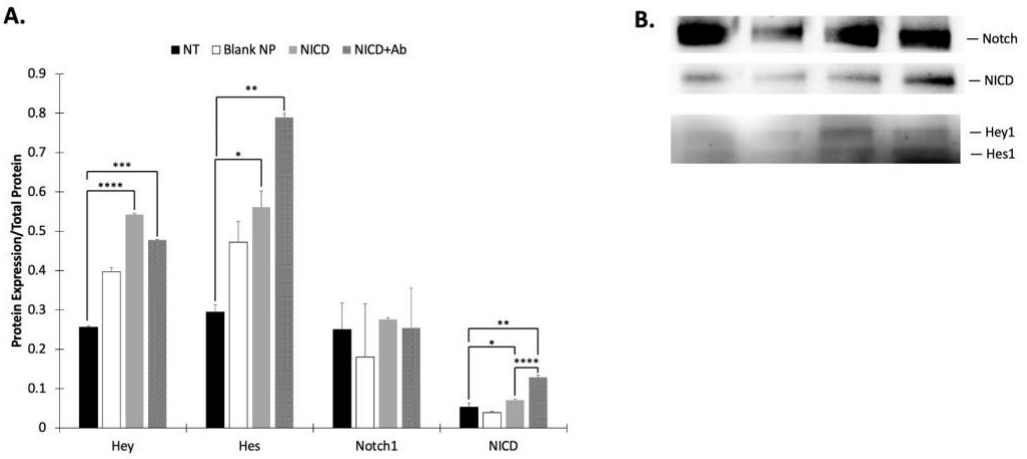

Figure 2.14: Western Blot analysis of Nanoparticle Treated HUVECs. *(A) Intensity analysis from western blot. * indicates ($p < 0.05$), ** ($p < 0.01$), *** ($p < 0.001$), **** ($p < 0.0001$) significance between groups. (B) Raw western blot images of Notch1, NICD, Hey1 and Hes1.*

2.4 Discussion

In this work, we have demonstrated the successful transfection of NICD plasmid to upregulated Notch signaling via PLGA nanoparticles. PLGA is one of the most characterized biopolymers with respect to drug delivery design and performance [79], which has been widely utilized for delivering proteins [65, 80-82] and hydrophobic drugs [83-86]. More recently, PLGA nanoparticle has been used as a delivery vehicles for gene delivery for vaccines [46], immunotherapy [43], or gene therapy [52, 76, 78, 87, 88]. Therefore, we have used PLGA for NICD DNA plasmid delivery to overcome the limitations of traditional viral vector methods such as negative immunological effects, random gene integration, base pair size restrictions, and cytotoxicity [89].

First, we optimized the molecular weight of the PLGA. Our data shows that the higher molecular weight, 55–65 kDa, PLGA was more cytocompatible, hemocompatible, and stable in various solutions. Even though the low molecular weight, 5–10 kDa, released the plasmid quickly, the nanoparticles were unstable in saline, a common liquid vehicle used for intravenous drug

delivery [86, 90-93]. Similarly, it has been shown that low molecular weight PLGA nanoparticles release the payload at a higher rate [94-96]. Therefore, the molecular weight can influence how long a drug of interest is released and exposed to the area of interest [95, 96]. These previous studies support our data showing that the low molecular weight releases the payload after 5 days. Interestingly, molecular weight differences of 5 kDa can have significantly different release profiles [94]. Additionally, lower molecular weight PLGA increases the pH of the surrounding fluid, which leads to cell death [97]. This would explain why at high concentrations, our lower molecular weight PLGA nanoparticles become significantly more toxic (**Figure 2.2C**). Mittal *et al.* showed that the poly-lactic acid to poly-glycolic acid ratio (PLA:PGA) have a significant effect of drug release as well [96]. Mittal *et al.* shows that the 50:50 composition allows for the highest release of the payload compared to 65:35 and 85:15 ratios [96]. They also show that *in vivo*, the higher molecular weight polymers allow for a higher cumulative drug in the blood stream in both oral and intravenous administration [96]. Additionally, others have shown that PLGA (50:50, 24-38 kDa) is non-toxic to cells with survival rates >90%, and hemolysis of <0.4% [98]. Our results support that of Thasneem *et al.* with cell viability of >90% at all tested concentrations for high molecular weight PLGA. We expanded that other molecular weights of PLGA, that are 10x lower and 2x higher than Thasneem's, have <0.3% hemolysis at all tested concentrations. Combining our data with those mentioned, PLGA is shown to be non-toxic, hemocompatible, and stable. Specifically, we show that higher molecular weight PLGA has superior performance over that of the low molecular weight PLGA, therefore, we have chosen the high molecular weight PLGA nanoparticles for antibody optimization.

As intravenous injection is the most common method to administer therapeutics, it is critical to ensure that the nanoparticle reaches its targeted destination. Although research reported

that encapsulated DNA into particles have modified their nanoparticles to be less toxic, have higher cellular uptake, or increase payload [53, 55, 99], there still is the limitation of off target delivery which causes systemic effects [100, 101]. For this reason, we investigated two endothelial cell specific antibodies, anti-EGFL7 and anti-Tie2+Tie1, on their ability to enhance cellular uptake in static and dynamic environments. We show that anti-Tie2+Tie1 has superior cellular uptake in both static and dynamic cell culture environments (**Figure 2.5 and Figure 2.10**). Additionally, we have demonstrated that compared to HL1 cells, there was significantly more cellular uptake of anti-Tie2+Tie1 conjugated nanoparticles in HUVECs, which is due to the fact that HL1 cells do not express Tie2 or Tie1 proteins [102] (**Figure 2.6C**). With our binding study, the anti-Tie2+Tie1 conjugated nanoparticles were bound significantly more than BSA conjugated or unconjugated nanoparticles. Additionally, the anti-Tie2+Tie1 nanoparticles bound significantly more to the Tie1+Tie2 coated slides than BSA-coated or uncoated slides (**Figures 2.6A, B**). Others have shown that even in cocultures of MCF-10A neoT and Caco-2, targeting antibodies for ductal breast carcinoma selectively target the MCF-10A neoT cells [103]. Unconjugated nanoparticles were up taken by both cell types in the coculture [103]. Other targeting nanoparticles have been able to repress expression of particular genes at a higher rate than the standard [93]. Compared to unconjugated nanoparticles, our targeting nanoparticles had significantly higher cellular uptake in the dynamic culture, supporting the notion that without targeting, the therapeutic clearance may diffuse the efficacy of the therapeutic.

In addition to site specific delivery, the encapsulated DNA needs to be bioactive. Others have shown that the sonication time or power, additives, or polymer molecular weight can affect the integrity of the plasmid [78]. We have shown that our synthesis method ensures plasmid delivery at several nanoparticle concentrations, and that the plasmid is bioactive. To find optimum

concentration of NICD to upregulate Notch signaling related genes, the 100 and 250 μg nanoparticle of NICD encapsulating nanoparticles significantly upregulated Notch target genes, *Hes1* and *Hey1*, compared to the gold standard lipofectamine with 5 μg of NICD (**Figure 2.10B**). We show that GFP protein can be synthesized in HUVECs by delivering the plasmid. Additionally, Notch and its related genes were quantified showing upregulation. However, in 500 and 1,000 μg nanoparticle groups, while NICD was also significantly upregulated, expression levels of target genes were downregulated. This indicates that the 100 μg or 250 μg of NICD nanoparticle concentrations were preferred to induce a downstream genetic effect although the higher concentrations were able to increase expression of NICD. Accordance with previous report, increment of NICD does not proportionally increase target gene expression levels [40] .

Although we demonstrated PLGA nanoparticles at HMW (55–65 kDa) are an appropriate material to deliver NICD plasmid to upregulate Notch signaling with *in vitro* flow experiment, we still need to evaluate our nanoparticle in an *in vivo* environment. Specifically, our *in vitro* experiment was limited in laminar flow, while *in vivo* injection of nanoparticle would be exposed to pulsatile blood flow environment. In future studies, we will optimize the NICD plasmid concentration, and the anti-Tie2+Tie1 concentration for conjugation to PLGA nanoparticles for upregulated Notch signaling in an animal model. This future experiment will help to translate our technology to effective therapeutic approach for translational medicine.

In this study, we have synthesized a PLGA nanoparticle that can deliver NICD plasmids to primary endothelial cells to upregulate Notch related components. In addition to being a nonviral transfection agent, the optimized nanoparticle was compatible with human cells and blood, and effectively delivered bioactive plasmid DNA to endothelial cells. These results demonstrate that

PLGA targeting nanoparticles could increase the genetic delivery in complex environments, such as *in vivo*, with minimal adverse effects.

2.5 Conclusions

Although we demonstrated PLGA nanoparticles at HMW (55–65 kDa) are an appropriate material to deliver NICD plasmid to upregulate Notch signaling with *in vitro* flow experiment, we still need to evaluate our nanoparticle in an *in vivo* environment. Specifically, our *in vitro* experiment was limited in laminar flow, while *in vivo* injection of nanoparticle would be exposed to pulsatile blood flow environment. In future studies, we will optimize the NICD plasmid concentration, and the anti-Tie2+Tie1 concentration for conjugation to PLGA nanoparticles for upregulated Notch signaling in an animal model. This future experiment will help to translate our technology to effective therapeutic approach for translational medicine.

In this study, we have synthesized a PLGA nanoparticle that can deliver NICD plasmids to primary endothelial cells to upregulate Notch related components. In addition to being a nonviral transfection agent, the optimized nanoparticle was compatible with human cells and blood, and effectively delivered bioactive plasmid DNA to endothelial cells. These results demonstrate that PLGA targeting nanoparticles could increase the genetic delivery in complex environments, such as *in vivo*, with minimal adverse effects.

In this work, we have shown that higher molecular weight PLGA outperforms the low molecular weight PLGA nanoparticles in cytotoxicity, cellular uptake, stability, and hemocompatibility. Additionally, the conjugation of anti-Tie2+Tie1 to the nanoparticles allows for a significant increase in endocytosis compared to those conjugated with anti-EGFL7. Lastly, our pCAG-GFP and TetO-FUW-NICD plasmids were both successfully encapsulated and

transfected into HUVECs. Most importantly, the plasmid was bioactive after transfection as indicated by GFP imaging and RT-PCR analysis. In conclusion, we can show that plasmid loaded nanoparticles have a higher transfection efficiency and create a significant genetic effect when applied to hard-to-transfect cells like HUVECs.

Chapter 3:

IN VIVO NANOPARTICLE ANALYSIS

3.1 Introduction

Since the early 2000s, more than 130 nanotechnology-based drug and delivery systems were in clinical or pre-clinical studies[104]. There have been numerous successes with differing delivery methods such as: oral, local, topical, and intravenous delivery[105]. In fact, each mode of delivery mentioned has at least one FDA approved nanoparticle drug or delivery system[106-109]. With the boom in nanotechnology, there is a greater need for more rigorous and meaningful pre-clinical studies using animal models.

The zebrafish (*danio rerio*) is gaining traction as a high throughput animal model that has easy maintenance, and a fast developmental stage compared to other vertebrate animal models[110, 111]. Additionally, many genes in the cardiac system and for development are highly conserved between humans and zebrafish[5, 16, 20, 111].

Zebrafish have a two chambered heart, one atrium and one ventricle. Despite this major structural difference, their electrocardiogram is extremely similar to that of a humans[112-114]. Zebrafish have the atrial depolarizing P-wave, ventricular depolarizing QRS complex, and the repolarizing T-wave. Also, zebrafish have a heart rate that is more similar to humans at 110-130 beats per minute (bpm) [115], compared to that of other small animal models such as mouse (310-840 bpm), rat (250-493 bpm), and rabbit (90-130 bpm)[116]. Additionally, cardiac genes between zebrafish and humans are highly conserved. There are many congenital heart defects that can be modeled in zebrafish to better understand the basic concepts of the genetic mutation[110]. Lastly, Smith *et al.* demonstrated that mutations in genes that were not previously

related to congenital heart defects, but were then evaluated in zebrafish, and showed that all 10 of the previously unrelated genes effected the atrioventricular canal, endothelial cushion, and valve malformations[110, 117].

Zebrafish are also a great model to evaluate toxicity of drugs or other treatments. In addition to being low cost and transparent, their small size allows for 96-well assays to be easily used. Also, the fish and human genome are highly conserved, zebrafish develop most organs with a week, and can survive severe cardiac mutations longer than mammals[110, 118]. Common malformations observed in zebrafish can be observed with a stereo microscope, enabling relatively easy assessment on the genetic toxicity of various treatments[104, 119, 120]. Lastly, due to the zebrafish transparency, the cardiac mechanics can be observed and imaged for further analysis.

In this study, we exposed zebrafish from 4 hpf to 96 hpf to varying concentrations of nanoparticles. A commonly used positive control of ZnO was utilized[104, 119, 120] to determine the statistical relevance of the genetic malformations. After injection, the cardiac mechanics were evaluated as well as the genetic expression of Notch1b and its related genes. Our data suggests that the PLGA nanoparticles are nontoxic and can successfully upregulate Notch1b and its related genes in an *in vivo* environment.

3.2 Experimental Section

3.2.1 Zebrafish Husbandry

Wild-type AB Zebrafish (Danio rerio) embryos were obtained under control of University of Texas at Arlington IACUC Embryos were collected within 1 hour of mating,

debris removed, and incubated at 27C in E3 media. Every 24 hours, the E3 media was exchanged, and unfertilized or dead embryos were removed.

3.2.2 Zebrafish Injection

Zebrafish larvae were harvested at 2 dpf and incubated in 0.003% Tricaine until larvae sedated to ensure proper anesthesia. The larvae were then placed in a 2% agarose E3 media mold laterally to visualize the heart and common cardinal vein (CVV). All nanoparticle solutions were at a concentration of 25 ug/mL in Saline (0.9% NaCl) and injected a total volume of 10 nL. Doxycycline was added to E3 media to induce translation of the TetO-FUW-NICD plasmid at a final concentration of 2 μg/mL.

3.2.3 *In Vivo* Biodistribution

Through zebrafish larval common cardinal vein (CCV), we have injected Coumarin 6-Loaded Anti-Tie2+Tie1 conjugated PLGA Nanoparticles suspended in saline. After 2 hours, 10x images were taken to observe the location of the nanoparticles if nanoparticles were successfully targeted in vascular system. Videos at 10x magnification were also taken, shown as representative stills, to depict nanoparticles in the circulatory system.

3.2.4 Nanoparticle Dosage & Toxicity Study

Fish embryos were harvested at 4-5 hpf. Then, empty PLGA nanoparticles at various concentrations (2, 10, 25, 50 μg/mL) were added to E3 media. E3 media alone served as a control. In a 12-well plate, 15 embryos were placed in each well with 1 mL of nanoparticle solution. At 24, 48, 72 and 96 hours post treatment, we performed blind study to observe the hatching rate, survival rate, and malformations of embryos at each developmental stage after injection different concentration. Malformations were the following: chorion with debris, delayed development, no

movement at 24 hours post treatment, pericardial edema, yolk sac edema, bent trunk, and tail malformations. At each time point, images were taken of each embryo for analysis. For the malformation analysis, four individuals were asked to rank the malformations on a scale from 0-2, where 0 is no malformation, 1 is the malformation is present, and 2 the malformation is severe. All traits were added together to show the overall malformation score. A fish was considered "hatched" if it had completely broken out of the chorion. The following equations were used for hatching rate and survival rate:

$$Hatching\ Rate = \frac{Number\ of\ Hatched\ Fish\ per\ Group}{Total\ Number\ of\ Fish\ in\ Group} \times 100\%$$

$$Survival\ Rate = \frac{Surviving\ Fish\ Per\ Group}{Total\ Number\ of\ Fish\ in\ Group} \times 100\%$$

3.2.5 Reverse Transcriptase Quantitative PCR

Zebrafish larvae were harvested at 2 dpf and injected into the CVV with the following groups: Saline (0.9% NaCl), or Saline & NICD-Loaded Anti-Tie2+Tie1 conjugated PLGA Nanoparticles. After 12 hours post injection (hpi), 24 hpi and 48 hpi, zebrafish were sacrificed with an overdose of Tricaine. The whole zebrafish was then homogenized by using the preset method "Elastic", and RNA isolated using Bio-Rad's Aurum Total RNA Mini Kit. cDNA was synthesized using Bio-Rad's iScript cDNA Synthesis kit. PCR was conducted in triplicate with the following primers:

Target	**Forward Primer**	**Reverse Primer**
zNICD	GCAGGATCCACCATGGGTTGTG GGGTGCTGCTGTCCCGCAAG	CTTGAATTCTTACTTAAATGCCTCTGGA ATGTGGGTG
zNotch1b	CAGAGAGTGGAGGCACAGTG CAATCC	GCCGTCCCATTCACACTCTGCATT
zDLL4	CAAAGTGGGAAGCAGACAGA GCTAAGG	CGGTCATCCCTGGGTGTGCATT
zHes1	GAGAGGCTGCCAAGGTTTTT	GTAATACGACTCACTATAGGGTCAAATAAA CTTCCCCAAAGGA

zHey1	AAACGTCGCAGAGGGATCAT	CCTGTTTCTCAAAGGCGCTG
zNrg1	GTGTGTTTGTCCCTGTGGACG CGT	CCTCCTGGAGCTTCCCCTCAAACA
zβ-Actin	CGAGCTGTCTTCCCATCCA	TCACCAACGTAGCTGTCTTTCTG

3.2.6 Cardiac Mechanical Performance

Zebrafish larvae were harvested at 2 dpf and injected into the CVV with the following groups: Saline (0.9% NaCl), Saline & Blank PLGA Nanoparticles, Saline & NICD-Loaded PLGA Nanoparticles, and Saline & NICD-Loaded Anti-Tie2+Tie1 conjugated PLGA Nanoparticles. After 48 hpi, zebrafish were anesthetized with 0.003% Tricaine for 10 minutes and placed in the 2% agarose E3 media mold laterally. The heart was visualized and viewed on a microscope at 4x magnification. Videos were taken in bright field of the heart for analysis of ejection fraction, heart rate, fractional shortening, end-systolic and -diastolic volume by deep-learning network.

3.2.7 Statistical Methods

All statistics were evaluated in the statistical program R unless otherwise noted. For the malformations, a one-way ANOVA was conducted followed by a Tukey test at each time point (24, 48, 72, or 96 hours). The survival test was conducted using GraphPad Prism 9.2.0. Bonferroni Correction was used to correct for multiple comparisons. RT-PCR results were evaluated using a one-way ANOVA per gene followed by a Tukey test. All p values lower than 0.05 were considered to be significant.

3.3 Results

3.3.1 Nanoparticle Dosage & Toxicity Study

Wild-type zebrafish embryos were exposed to HMW PLGA nanoparticles at varying concentrations from 2 μg/mL to 50 μg/mL, ZnO nanoparticles at 10 μg/mL, or no treatment. After 24 hours, there was a significant difference in hatching rate between all groups and the ZnO nanoparticles. Additionally, all groups were significantly different from the no treatment group at 24 hours. As time passed, the nanoparticles seemed to induce hatching, as seen at 48, 72, and 96 hours, each concentration of PLGA nanoparticles had a higher hatching rate (**Figure 3.1**).

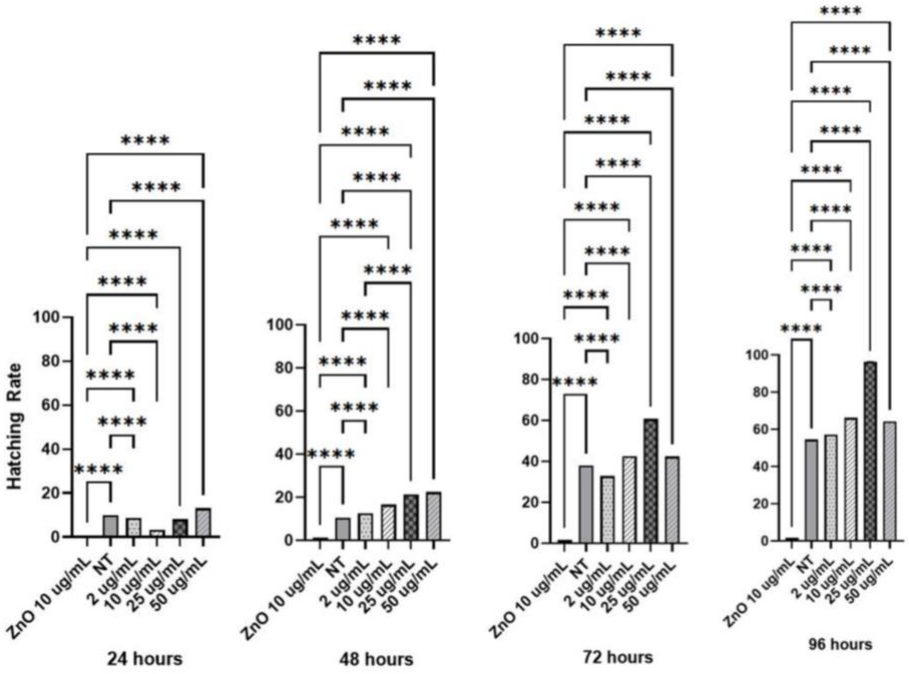

Figure 3.1: Hatching and Survival Rates for embryonic zebrafish toxicity study*. (A) Hatched to Unhatched ratio of nontreated fish to various concentrations of empty PLGA nanoparticle solutions. (B) Live to Dead ration of nontreated fish to treated fish at various time points. **** indicates a (p < 0.0001), n = 105 fish per group.*

Zebrafish survival was also measured every 24 hours. The ZnO nanoparticles caused a significant decrease in survival rate compared to the PLGA nanoparticles (**Figure 3.2**). Additionally, the highest nanoparticle concentration, 50 μg/mL, had a large loss at 24 hours

compared to other groups. Compared to the no treatment group, the PLGA nanoparticles did not seem to cause a significant effect.

Many malformations were observed in the zebrafish embryos over time including chorion debris, delayed development, pericardial edema, yolk sac edema, bent trunk, and tail malformations. Within the first 24 hours, there was no difference between each group when observing chorion debris. However, the PLGA nanoparticle groups had significantly less chorion debris than the positive control, ZnO nanoparticles (**Figure 3.3**). The nanoparticles also showed significantly less developmental delay at 24, 72, and 96 hours compared to the ZnO nanoparticles (**Figure 3.4**). There was also less significant pericardial edema and yolk sac edema in the PLGA nanoparticle treated groups than the ZnO group. However, at 48 hours the 50 μg/mL PLGA nanoparticle group was not significantly different from the positive control in both yolk sac and pericardial edema (**Figures 3.5 and 3.6**). The nanoparticle treatment also did not cause significantly less bent trunk malformation compared to the ZnO nanoparticles (**Figure 3.7**). However, the 50 μg/mL was not significantly different from the ZnO particles at 48 and 72 hours. This could indicate that there is some toxicity at this concentration. By 96 hours of exposure, the zebrafish larvae did not have a significant difference between any of the groups. The PLGA nanoparticles had significantly fewer tail malformations compared to the ZnO group (**Figure 3.8**).

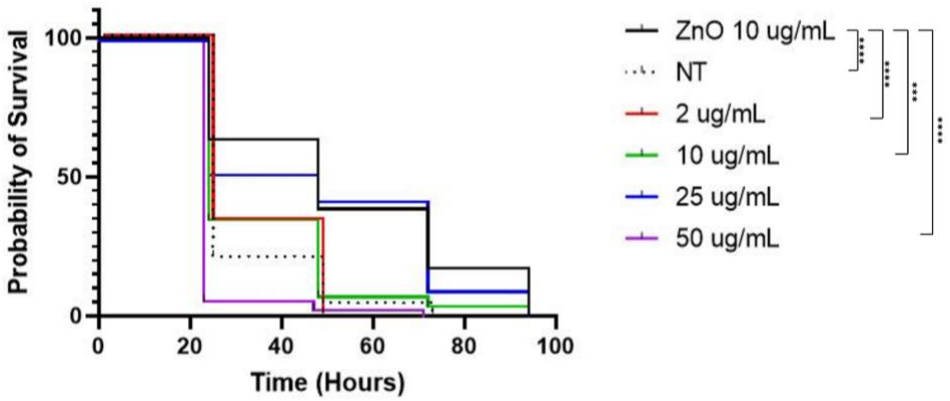

Figure 3.2: Survival of Zebrafish embryos. *Exposure to HMW PLGA nanoparticles at various concentrations, ZnO nanoparticles at 10 ug/mL, or no treatment. *** indicates ($p < 0.001$), **** indicates ($p < 0.0001$), n = 105 fish per group.*

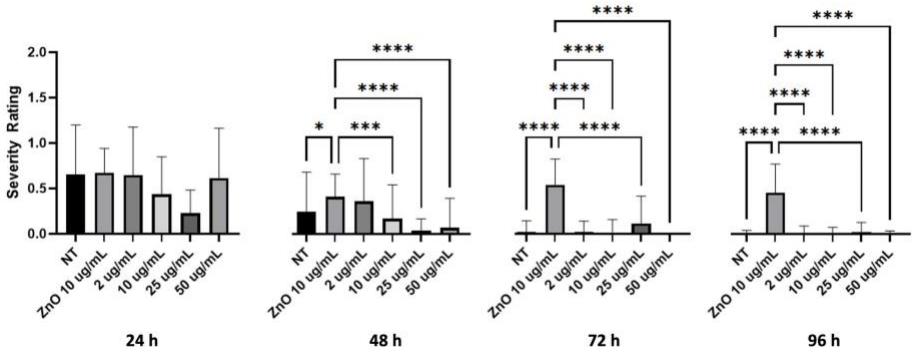

Figure 3.3: Chorion Debris formation on zebrafish embryos. *Chorion debris was rated 0, 1, or 2 based on the severity of the debris every 24 hours. * indicates ($p < 0.05$), *** indicates ($p < 0.001$), **** indicates ($p < 0.0001$) between each group.*

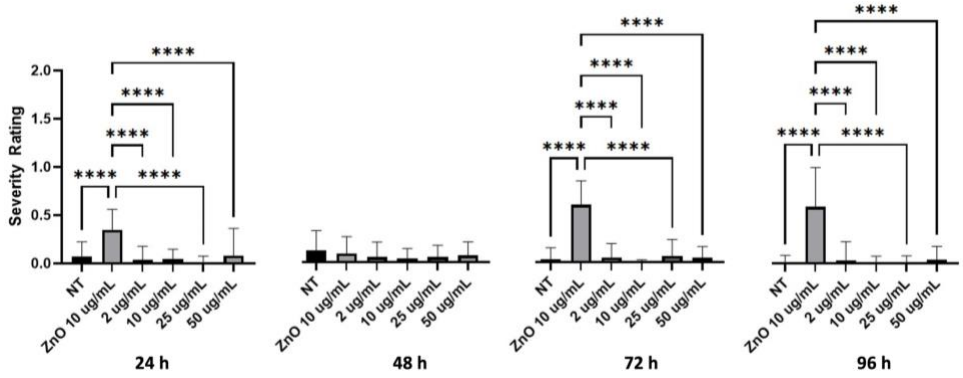

Figure 3.4: Developmental delays in zebrafish exposed to various concentrations of PLGA nanoparticles*. Data shown at mean ± standard deviation. * indicates ($p < 0.05$) and ** indicates ($p < 0.01$) a significant difference between groups, n = 70.*

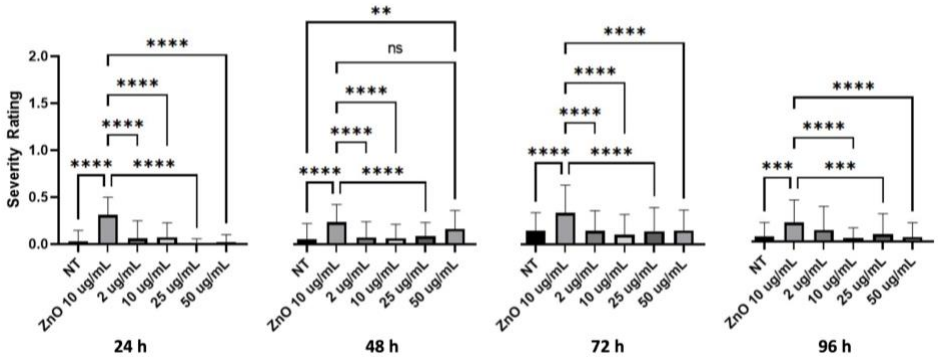

Figure 3.5: Pericardial edema after nanoparticle exposure. *Data shown at mean ± standard deviation. * indicates ($p < 0.05$), ** indicates ($p < 0.01$), and *** indicates a significant value of ($p < 0.001$), n = 70.*

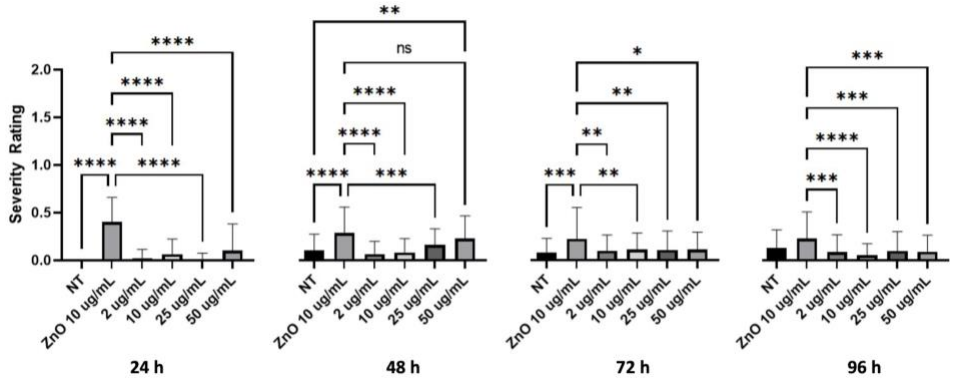

Figure 3.6: Yolk sac edema after PLGA nanoparticle exposure. *Data shown at mean ± standard deviation. * indicates ($p < 0.05$) and **** indicates a significant value of ($p < 0.0001$), n = 70.*

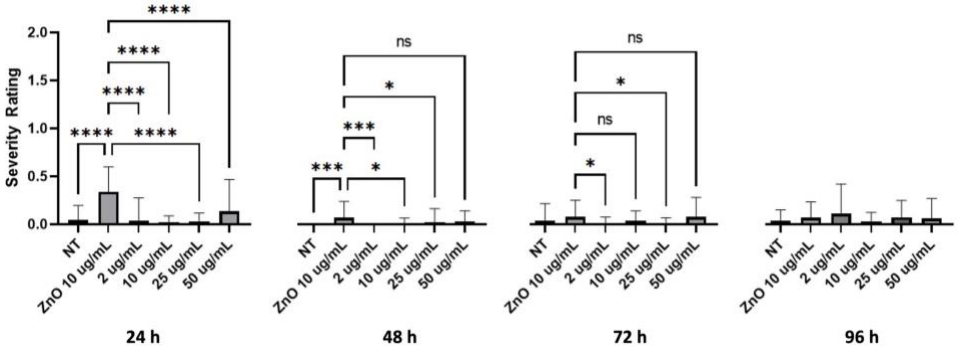

Figure 3.7: Development of bent trunk after nanoparticle exposure. *Data shown at mean ± standard deviation. * indicates ($p < 0.05$), *** indicates a significant value of ($p < 0.001$), n = 70.*

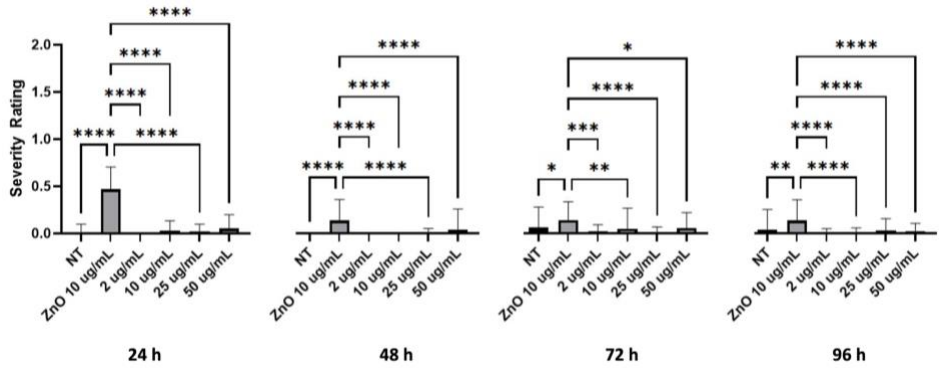

Figure 3.8: Tail malformation after nanoparticle exposure. *Data shown at mean ± standard deviation. * indicates a significant value of ($p < 0.05$), n = 70.*

3.3.2 Biodistribution of PLGA Nanoparticles

After injection and recovery, zebrafish were imaged under 10x magnification. The nanoparticles were easily observed as fast-moving particles in the blood stream (**Figure 3.9A**). By 2 hours, small clusters of nanoparticles have been uptaken by the zebrafish (**Figure 3.9B**). Rolling nanoparticles could be seen as long streaks on the walls of the vessel. Uptaken nanoparticles were depicted as stationary fluorescent clusters (**Figure 3.9B**, yellow arrows).

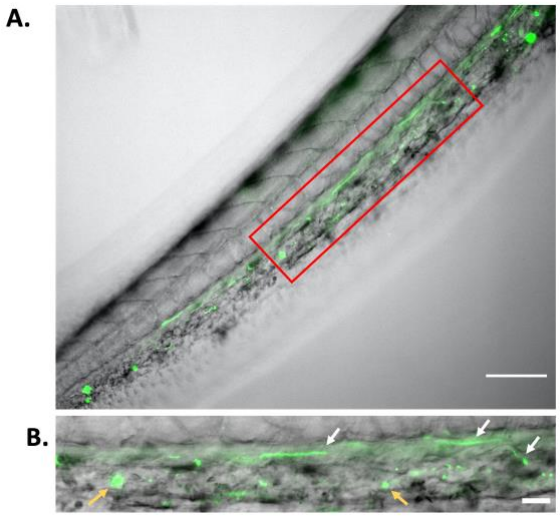

Figure 3.9: Coumarin-6 Loaded Nanoparticles after Injection. *(A) Coumarin-6 nanoparticles traveling in the caudal artery of the zebrafish tail. Red box is blown up and shown as (B). White arrows show nanoparticles rolling along vessel walls. Yellow arrows indicate clusters of endocytosed nanoparticles.*

The fluorescent nanoparticles could be seen traveling down the tail via the dorsal aorta into the caudal artery, into the caudal vein, and up the posterior cardinal vein. Nanoparticles were also able to enter the capillaries and travel into the deeper tissues (**Figure 3.10**). As the blood velocity slows down, the nanoparticle also travels at a slower speed (**Figure 3.10**, 1.6s – 4.8s). Once the nanoparticle neared the posterior cardinal vein, the nanoparticle speed increased.

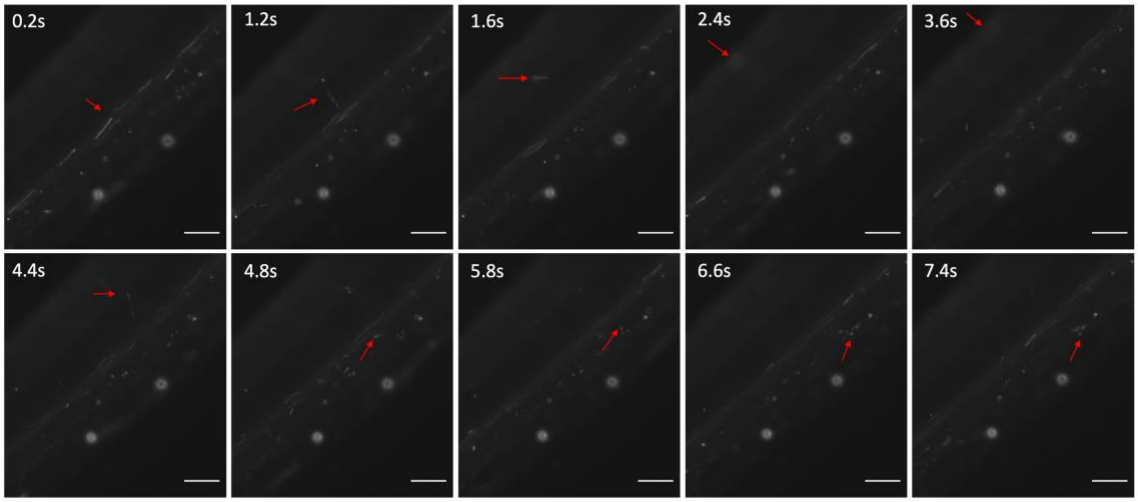

Figure 3.10: Coumarin-6 Nanoparticle Traveling in Vessel. *Representative stills from Supplementary Video1 showing nanoparticles traveling from the caudal artery (0.2 – 1.2s), into the capillaries of the tail tissue (1.6s – 4.8s), and entering the posterior caudal vein (6.6s – 7.4s).*

The coumarin-6 nanoparticles were also visible in the zebrafish heart. The nanoparticles could be seen rolling along the endocardium and the heart beat (**Figure 3.11**). As the nanoparticle observed bound more tightly to the endocardium, the nanoparticle slowed its speed (**Figure 3.11**, 3.0s – 5.0s). However, the nanoparticle was not taken up and was flown through the rest of the fish.

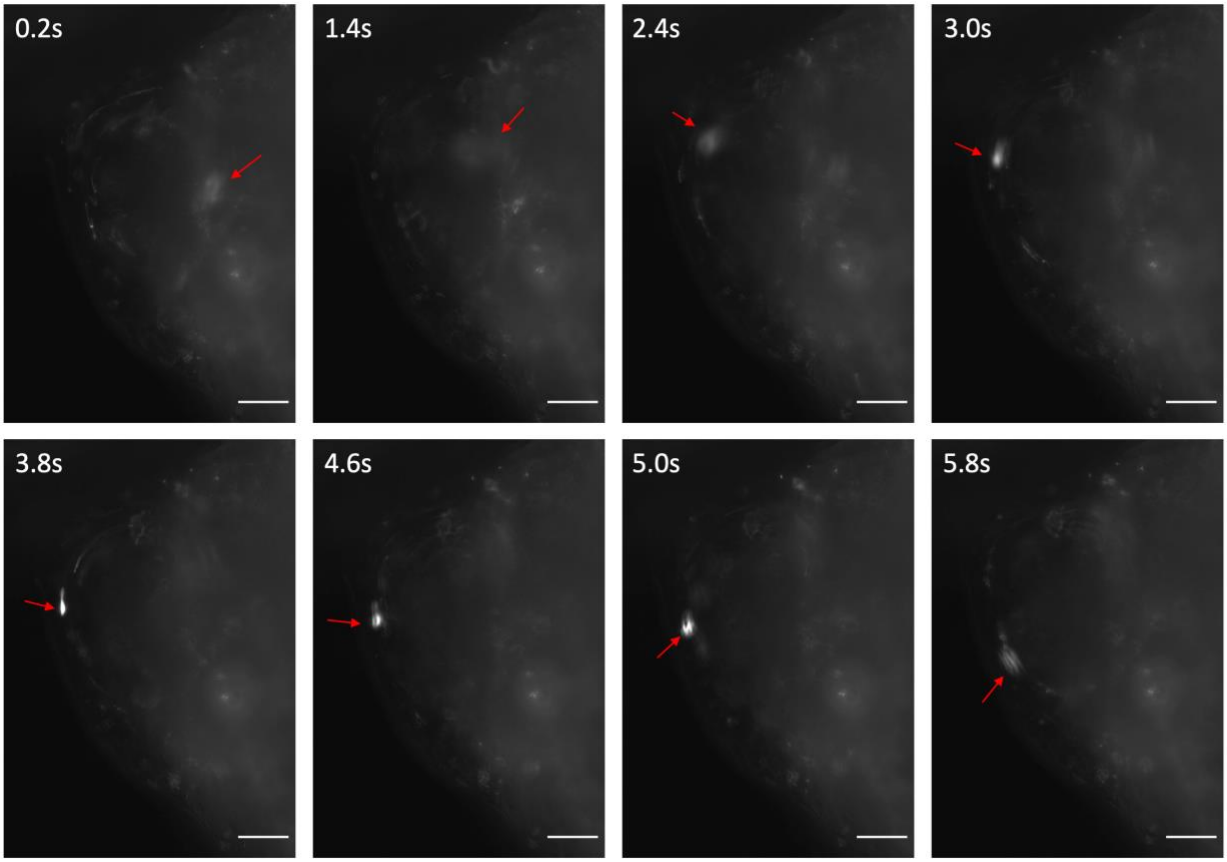

Figure 3.11: Coumarin-6 Nanoparticles Rolling on Endocardium. *Representative stills from Supplementary Video2 showing nanoparticles flowing through the cardiac chambers.*

3.3.3 Reverse Transcriptase Quantitative PCR

Zebrafish were injected with 10 nL of 25 μg/mL of PLGA nanoparticles at 2 dpf into the common cardinal vein. The groups consisted of NICD-loaded Anti-Tie2+Tie1-conjugated nanoparticles, or Saline injection. The NICD loaded nanoparticles had significantly higher expression of all genes, except DLL4 at 12 hpi, at each time point compared to the saline injection. Additionally, gene expression peaked at 24 hours post injection for all genes observed. However, after 48 hours Notch1b and Hey1 returned to insignificant levels. Nrg1 continued to show significantly higher expression after 48 hours post injection compared to saline. Lastly, NICD was significantly higher at 48 hours, implying that the nanoparticle was still releasing NICD plasmid from its core.

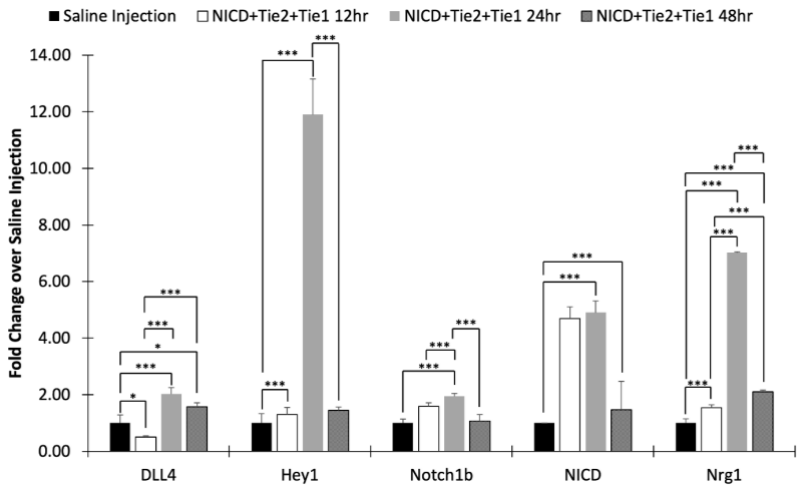

Figure 3.12: Genetic expression of Notch related genes after NICD-loaded anti-Tie2+Tie1 conjugated PLGA nanoparticles were injected. *At 12, 24, and 48 hours post injection, Hey1, Notch1b, NICD, and Nrg1were significantly upregulated compared to the saline injection control. The peak expression for both Notch1b and its' downstream genes was at 24 hours post injection.*

3.3.4 Cardiac Mechanical Performance

The cardiac performance was evaluated using a deep learning algorithm, previously reported[121]. Here, the dice loss coefficient plateaus at 0.18, indicating that the model ____accurately? Predicts the zebrafish heart shape (**Figure 3.13A**). Additionally, the Intersection of Union (IoU) score reaches 0.80, indicating_____ (**Figure 3.13B**).

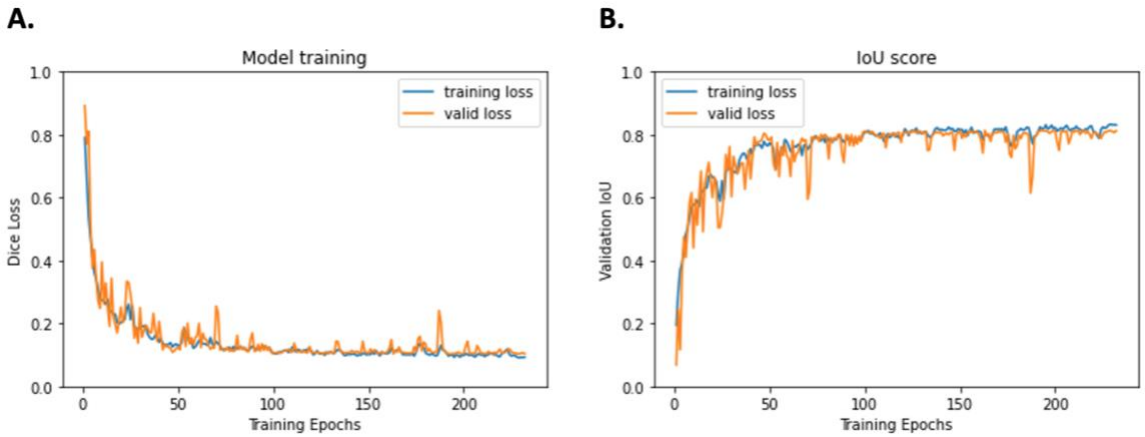

Figure 3.13: Cardiac Model Performance. *(A) Graph showing that over 250 training data sets, the Dice Loss value plateaus at 1.8. (B) Intersection of Union Score indicating the accuracy of the model's predictive abilities.*

The model can be qualitatively compared to show that the model prediction, Figure 3.14 Column 3, is similar to the hand segmented volume, Figure 3.14 Column 2.

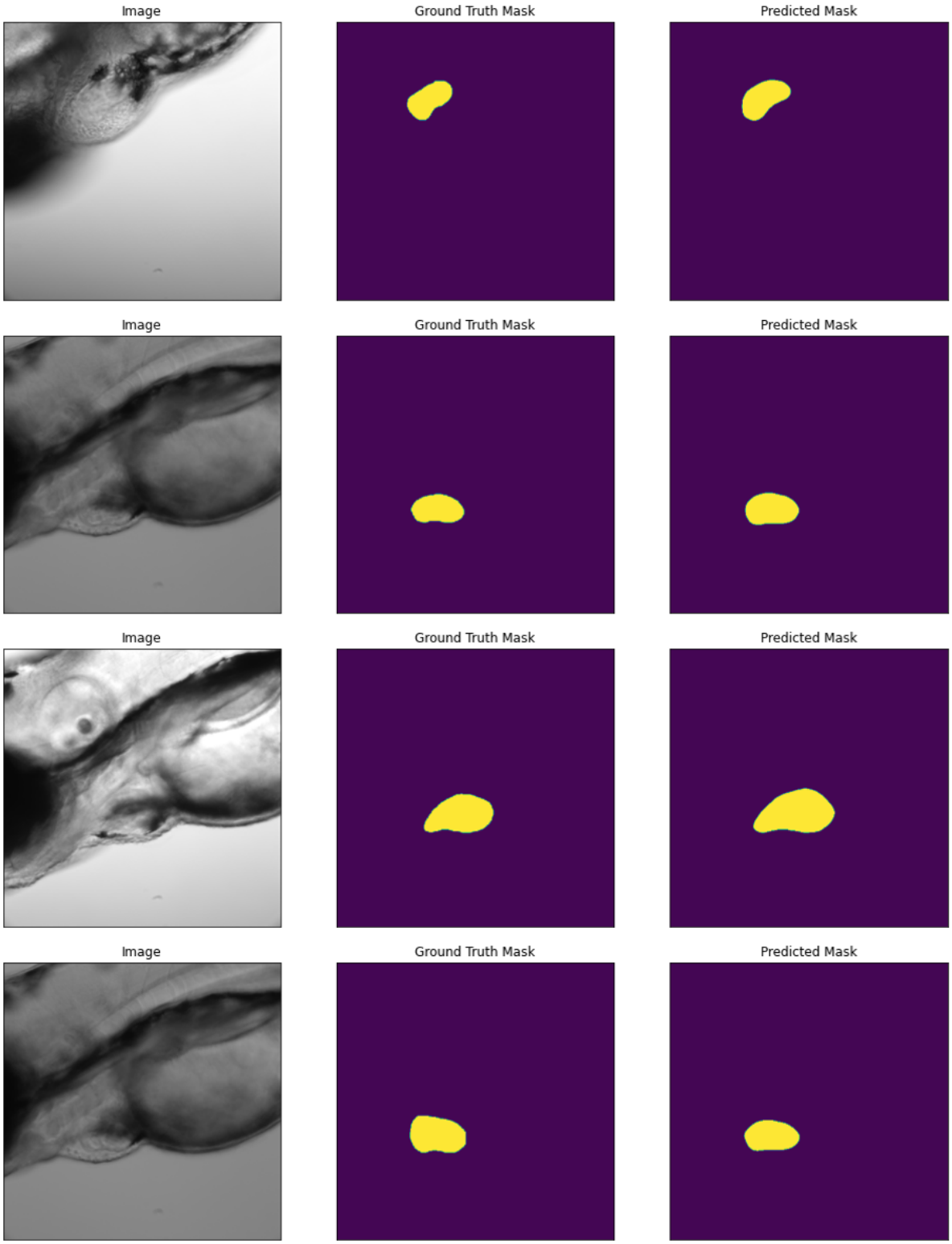

Figure 3.14: Representative Images of Model Output. *Representative images of the image input (column 1), hand segmented cardiac volume (column 2), and the model's predicted cardiac volume (column 3).*

From the model, we were able to find the End Systolic Area (ESA), End Diastolic Area (EDA), Ejection Fraction (EF), and Fractional Shortening (FS) (**Table 3.13**). We found that the NICD Plasmid injected fish had a larger ESA and EDA, although it was not significant. However, the EF and FS remained similar.

Table 3.1: Cardiac Performance.

	End Systolic Area	End Diastolic Area	Ejection Fraction	Fractional Shortening
NICD Injected Fish	28,032 ± 19,636	39,817 ± 29,277	0.284 ± 0.066	0.1640 ± 0.1519
Saline Injected Fish	19,317 ± 6,526	25,054 ± 5,166	0.242 ± 0.098	0.1637 ± 0.0506

3.4 Discussion

Zebrafish embryos were collected and observed over time to evaluate the toxicity, hatching rate, and survival when exposed to various concentrations of PLGA nanoparticles, ZnO nanoparticles as positive control, or no treatment. The 50 μg/mL concentration of nanoparticles caused a large decrease in survival after 24 hours, compared to other groups. However, the lower concentration of nanoparticles showed no significant difference to the negative control, showing that they do not affect survival. The nanoparticles do affect the hatching rate and seem to induce hatching as seen by the significant increase in hatching compared to the negative control (**Figure 3.1**).

PLGA nanoparticles had no significant difference between the negative control for the chorion debris, developmental delay, pericardial and yolk sac edema. However, the 50 μg/mL nanoparticle group did have significant pericardial and yolk sac edema at 48 hours post exposure (**Figure 3.5, 3.6**). The edemas did return to normal after 96 hours of exposure. The edemas could signify that the nanoparticle concentration was too high, which resulted in abnormal defects. As

the fish grew stronger, they seemed to be able to handle the larger dosage which resulted in the reduction of the edemas. Similarly, the embryos developed a bent trunk at 48 and 72 hours post exposure, which could be another indication of toxicity. However, at 96 hours the fish had no significant bent trunk malformations.

Injection of the targeting nanoparticles proved efficient in upregulating Notch1b and its related genes. As early as 12 hours post injection, there was a significant increase in Hey1, Notch1b, NICD and Nrg1 genes. At 24 hours, all genes were significantly upregulated. The intense upregulation of Notch1b and its related genes could be due to the burst release of plasmid or dye shown earlier (**Figure 2.2, 2.8, 2.9A**). The similarities indicate that our model drug and release profiles from Chapter 2 are effective in predicting the outcome *in vivo*. Additionally, our western blot are RT-PCR results (**Figures 2.11, 2.12**) are mirrored in the upregulation of the same genes in the zebrafish model.

One potential reason as to why DLL4 was not upregulated at 12 hpi could be due to the fact that it is upstream of Notch1b. The amount of time for the feedback loop to return to the beginning could not have been sufficient at 12 hours. However, at 24 hours DLL4 is significantly upregulated, indicating that all portions of the Notch loop have been affected. By the NICD plasmid-loaded nanoparticles.

As early as 2 hpi, nanoparticles can be seen stationary in the zebrafish vessel walls (**Figure 3.10**). Additionally, the nanoparticles can be seen rolling on the vessel walls of the caudal artery. Due to the slower nanoparticle speed, one can observe when the nanoparticle exits the caudal artery, enters the capillaries, and enters the caudal vein (**Figure 3.11**). Nanoparticle rolling can also be observed in the cardiac chamber (**Figure 3.12**). The nanoparticle in focus slows down its velocity as it interacts with the endocardium.

Comparing the cardiac performance between saline injected fish and NICD plasmid injected fish, one can see that there is no significant difference in any of the measured functions (**Table 3.1**). Additionally, others have shown similar controls for EF and FS, indicating that the deep learning model is comparable to published methods [19, 20, 122-124]. Similarly, Lee *et al.* showed that after increasing the viscosity of the blood – via EPO mRNA injection or isoproterenol – that there was no significant difference in Notch signaling between that and the control [19].

3.5 Conclusions

In this study, we have shown that PLGA nanoparticles at low concentrations do not show significant physical abnormalities at each time point tested. The nanoparticles did induce a significant increase in hatching, but this did not seem to affect the survival rate of the larvae. Additionally, after successful injection of the targeting nanoparticles, we were able to demonstrate that the treatment significantly upregulated Notch1b and its related genes at 25 μg/mL. The nanoparticles could be observed rolling on the caudal artery and the endocardium, possibly interacting with the Tie1 or Tie2 proteins expressed in those cells. Lastly, addition of NICD plasmid did not significantly affect the cardiac mechanical performance, which was similarly shown in others' work.

Chapter 4:

CONCLUSIONS

The highly conserved Notch signaling pathway is involved in tissue development and regeneration of the cardiac, neuronal, immune and endocrine systems [15, 16, 21-28]. Notch also regulates the arteriovenous specification and differentiation in endothelial and vascular smooth muscle cells during vessel sprouting, branching during normal and pathological angiogenesis, and the physiological responses of vascular smooth muscle cells [15, 16, 18, 25, 38, 39]. Since it is involved in myriad of tissues, a small defect can have substantial consequences such as Left Ventricular Noncompaction or Alagille Syndrome.

We have created a nanovehicle that can successfully deliver the Notch Intracellular Domain to endothelial cells that could have compromised Notch signaling. We synthesized Poly(lactic-co-glycolic) acid nanoparticles with molecular weights of 1-5 kDa and 55-65 kDa. We evaluated the particles based on their morphology, cytocompatibility, hemocompatibility, and gene delivery. We have determined that the high molecular weight nanoparticles are an appropriate material to delivery NICD plasmid to upregulate Notch signaling in our *in vitro* experiments. Additionally, we emphasized the importance of the flow studies, demonstrating that the targeting antibody increases specific uptake into endothelial cells.

We have also shown that our nonviral transfection nanoparticle can successfully deliver bioactive NICD and GFP plasmid to primary human endothelial cells. We encapsulated TetO-FUW-NICD or pCAG-GFP plasmids into the high molecular weight PLGA nanoparticles and observed the plasmid burst release. Importantly, we successfully determined that the NICD plasmid could enhance downstream Notch molecules via our RT-PCR.

To further demonstrate the translational abilities of our nanoparticle, we conducted *in vivo* experiments using zebrafish as an animal model. We have shown that our PLGA nanoparticles do not show significant physical abnormalities at various stages of development. Additionally, our nanoparticles did not significantly affect the survival rate of the larvae. After successful injection of our nanoparticles, we observed upregulation of Notch1b and its related genes at 25 μg/mL. We also observed nanoparticles rolling along the endocardium and caudal artery of the zebrafish. This possibly could indicate the positive interactions between Tie1 or Tie2 proteins interacting with the anti-Tie2+Tie1 conjugated nanoparticles.

Chapter 5:
REFERENCES

[1] S. Tu and N. C. Chi, "Zebrafish models in cardiac development and congenital heart birth defects," *Differentiation; research in biological diversity,* vol. 84, no. 1, pp. 4-16, 06/15 2012, doi: 10.1016/j.diff.2012.05.005.

[2] L. A. Samsa, B. Yang, and J. Liu, "Embryonic Cardiac Chamber Maturation: Trabeculation, Conduction and Cardiomyocyte Proliferation," *American journal of medical genetics. Part C, Seminars in medical genetics,* vol. 163, no. 3, pp. 157-168, 05/29 2013, doi: 10.1002/ajmg.c.31366.

[3] A. S. Go *et al.*, "Heart disease and stroke statistics--2013 update: a report from the American Heart Association," *Circulation,* vol. 127, no. 1, pp. e6-e245, Jan 1 2013, doi: 10.1161/CIR.0b013e31828124ad.

[4] J. R. Hove, R. W. Koster, A. S. Forouhar, G. Acevedo-Bolton, S. E. Fraser, and M. Gharib, "Intracardiac fluid forces are an essential epigenetic factor for embryonic cardiogenesis," *Nature,* 10.1038/nature01282 vol. 421, no. 6919, pp. 172-177, 01/09/print 2003, doi: http://www.nature.com/nature/journal/v421/n6919/suppinfo/nature01282_S1.html.

[5] C. Peshkovsky, R. Totong, and D. Yelon, "Dependence of cardiac trabeculation on neuregulin signaling and blood flow in zebrafish," *Developmental Dynamics,* vol. 240, no. 2, pp. 446-456, 2011, doi: 10.1002/dvdy.22526.

[6] J. Liu *et al.*, "A dual role for ErbB2 signaling in cardiac trabeculation," *Development (Cambridge, England),* vol. 137, no. 22, pp. 3867-3875, 09/20/accepted 2010, doi: 10.1242/dev.053736.

[7] N. Baeyens, C. Bandyopadhyay, B. G. Coon, S. Yun, and M. A. Schwartz, "Endothelial fluid shear stress sensing in vascular health and disease," *J Clin Invest,* vol. 126, no. 3, pp. 821-8, Mar 1 2016, doi: 10.1172/JCI83083.

[8] T. G. Hoog, S. J. Fredrickson, C. W. Hsu, S. M. Senger, M. E. Dickinson, and R. S. Udan, "The effects of reduced hemodynamic loading on morphogenesis of the mouse embryonic heart," *Dev Biol,* Jul 17 2018, doi: 10.1016/j.ydbio.2018.07.007.

[9] T. Bartman and J. Hove, "Mechanics and function in heart morphogenesis," *Developmental Dynamics,* vol. 233, no. 2, pp. 373-381, 2005, doi: 10.1002/dvdy.20367.

[10] P. Teekakirikul, M. A. Kelly, H. L. Rehm, N. K. Lakdawala, and B. H. Funke, "Inherited cardiomyopathies: molecular genetics and clinical genetic testing in the postgenomic era," *J Mol Diagn,* vol. 15, no. 2, pp. 158-70, Mar 2013, doi: 10.1016/j.jmoldx.2012.09.002.

[11] A. F. M. Moorman and V. M. Christoffels, "Cardiac Chamber Formation: Development, Genes, and Evolution," *Physiological Reviews,* vol. 83, no. 4, pp. 158-170, Oct 2003, doi: 10.1152/physrev.00006.2003.

[12] B. C. Weiford, V. D. Subbarao, and K. M. Mulhern, "Noncompaction of the ventricular myocardium," *Circulation,* vol. 109, no. 24, pp. 2965-71, Jun 22 2004, doi: 10.1161/01.CIR.0000132478.60674.D0.

[13] R. Jenni, E. N. Oechslin, and B. van der Loo, "Isolated ventricular non-compaction of the myocardium in adults," *Heart,* vol. 93, no. 1, pp. 11-5, Jan 2007, doi: 10.1136/hrt.2005.082271.

[14] N. C. Chi *et al.*, "Genetic and Physiologic Dissection of the Vertebrate Cardiac Conduction System," *PLOS Biology,* vol. 6, no. 5, p. e109, 2008, doi: 10.1371/journal.pbio.0060109.
[15] G. D'Amato, G. Luxán, and J. L. de la Pompa, "Notch signalling in ventricular chamber development and cardiomyopathy," *The FEBS Journal,* vol. 283, no. 23, pp. 4223-4237, 2016, doi: 10.1111/febs.13773.
[16] F. A. High and J. A. Epstein, "The multifaceted role of Notch in cardiac development and disease," *Nature Reviews,* vol. 9, no. 1, pp. 49-61, 2008, doi: http://dx.doi.org/10.1038/nrg2279.
[17] U. Teichmann and M. Kessel, "Highly restricted BMP10 expression in the trabeculating myocardium of the chick embryo," *Dev Genes Evol,* vol. 214, no. 2, pp. 96-8, Feb 2004, doi: 10.1007/s00427-003-0380-2.
[18] R. Diaz-Trelles *et al.*, "Notch-independent RBPJ controls angiogenesis in the adult heart," *Nat Commun,* vol. 7, p. 12088, Jun 30 2016, doi: 10.1038/ncomms12088.
[19] J. Lee *et al.*, "Spatial and temporal variations in hemodynamic forces initiate cardiac trabeculation," *JCI Insight,* vol. 3, no. 13, Jul 12 2018, doi: 10.1172/jci.insight.96672.
[20] J. Lee *et al.*, "4-Dimensional light-sheet microscopy to elucidate shear stress modulation of cardiac trabeculation," *The Journal of Clinical Investigation,* vol. 126, no. 5, pp. 1679-1690, 05/02/ 2016, doi: 10.1172/JCI83496.
[21] N. Chadwick, M. C. Nostro, M. Baron, R. Mottram, G. Brady, and A. M. Buckle, "Notch signaling induces apoptosis in primary human CD34+ hematopoietic progenitor cells," *Stem Cells,* vol. 25, no. 1, pp. 203-10, Jan 2007, doi: 10.1634/stemcells.2005-0303.
[22] M. D. Chau, R. Tuft, K. Fogarty, and Z. Z. Bao, "Notch signaling plays a key role in cardiac cell differentiation," *Mech Dev,* vol. 123, no. 8, pp. 626-40, Aug 2006, doi: 10.1016/j.mod.2006.06.003.
[23] C. E. Challice and S. Viragh, "The Architectural Development of the Early Mammalian Heart," *Tissue and Cell,* vol. 6, no. 3, pp. 447-462, 2005, doi: https://doi.org/10.1016/0040-8166(74)90037-8.
[24] S. Da'as, A. J. Coombs, T. B. Balci, C. A. Grondin, A. A. Ferrando, and J. N. Berman, "The zebrafish reveals dependence of the mast cell lineage on Notch signaling in vivo," *Blood,* vol. 119, no. 15, pp. 3585 - 3594, 2019, doi: 10.1182/blood-2011-10-.
[25] J. L. de la Pompa and J. A. Epstein, "Coordinating tissue interactions: Notch signaling in cardiac development and disease," *Dev Cell,* vol. 22, no. 2, pp. 244-54, Feb 14 2012, doi: 10.1016/j.devcel.2012.01.014.
[26] A. Raya *et al.*, "Activation of Notch signaling pathway precedes heart regeneration in zebrafish," *Proc Natl Acad Sci U S A,* vol. 100 Suppl 1, pp. 11889-95, Sep 30 2003, doi: 10.1073/pnas.1834204100.
[27] E. Gazave *et al.*, "Origin and evolution of the Notch signalling pathway: an overview from eukaryotic genomes," *BMC Evol Biol,* vol. 9, p. 249, Oct 13 2009, doi: 10.1186/1471-2148-9-249.
[28] G. S. Richards and B. M. Degnan, "The Dawn of Developmental Signaling in the Metazoa," *Cold Spring Harb Symp Quant Biol,* no. 74, pp. 81-90, 2009, doi: 10.1101/sqb.2009.74.028.
[29] A. Engler, R. Zhang, and V. Taylor, *Molecular Mechanisms of Notch Signaling* (Advances in Experimental Medicine and Biology). Springer, Cham, 2018.

[30] R. Kopan and M. X. Ilagan, "The canonical Notch signaling pathway: unfolding the activation mechanism," *Cell,* vol. 137, no. 2, pp. 216-33, Apr 17 2009, doi: 10.1016/j.cell.2009.03.045.
[31] C. Wilson, J. Kavaler, and S. T. Ahmad, "Expression of a human variant of CHMP2B linked to neurodegeneration in Drosophila external sensory organs leads to cell fate transformations associated with increased Notch activity," *Dev Neurobiol,* vol. 80, no. 3-4, pp. 85-97, Mar 2020, doi: 10.1002/dneu.22722.
[32] M. Garis and L. A. Garrett-Sinha, "Notch Signaling in B Cell Immune Responses," *Front Immunol,* vol. 11, p. 609324, 2020, doi: 10.3389/fimmu.2020.609324.
[33] M. Dell'Aringa and R. L. Reinhardt, "Notch signaling represents an important checkpoint between follicular T-helper and canonical T-helper 2 cell fate," *Mucosal Immunol,* vol. 11, no. 4, pp. 1079-1091, Jul 2018, doi: 10.1038/s41385-018-0012-9.
[34] D. Huang and R. Wang, "Exploring the mechanism of pancreatic cell fate decisions via cell-cell communication," *Mathematical Biosciences and Engineering,* vol. 18, no. 3, pp. 2401-2424, 2021, doi: 10.3934/mbe.2021122.
[35] E. D. Bankaitis, M. E. Bechard, G. Gu, M. A. Magnuson, and C. V. E. Wright, "ROCK-nmMyoII, Notch and Neurog3 gene-dosage link epithelial morphogenesis with cell fate in the pancreatic endocrine-progenitor niche," *Development,* vol. 145, no. 18, Sep 21 2018, doi: 10.1242/dev.162115.
[36] Z. Lu, H. Liu, L. Xue, P. Xu, T. Gong, and G. Hou, "An activated Notch1 signaling pathway inhibits cell proliferation and induces apoptosis in human esophageal squamous cell carcinoma cell line EC9706," *International Journal of Oncology,* vol. 32, pp. 643-651, 2007, doi: https://doi.org/10.3892/ijo.32.3.643.
[37] M. D. L. Chau, R. Tuft, K. Fogarty, and Z.-Z. Bao, "Notch Signaling plays a key role in cardiac cell differentiation," *Mechanisms of Development,* vol. 123, pp. 626-640, 2006, doi: 10.1016/j.mod.2006.06.003.
[38] G. Luxán *et al.*, "Mutations in the NOTCH pathway regulator MIB1 cause left ventricular noncompaction cardiomyopathy," *Nature Medicine,* Article vol. 19, p. 193, 01/13/online 2013, doi: 10.1038/nm.3046
https://www.nature.com/articles/nm.3046#supplementary-information.
[39] M. Nemir and T. Pedrazzini, "Functional role of Notch signaling in the developing and postnatal heart," *Journal of Molecular and Cellular Cardiology,* vol. 45, no. 4, pp. 495-504, 2008/10/01/ 2008, doi: http://dx.doi.org/10.1016/j.yjmcc.2008.02.273.
[40] K. I. Baek *et al.*, "Ultrafine Particle Exposure Reveals the Importance of FOXO1/Notch Activation Complex for Vascular Regeneration," *Antioxidants & redox signaling,* vol. 28, no. 13, pp. 1209-1223, May 1 2018, doi: 10.1089/ars.2017.7166.
[41] B. R. Meade and S. F. Dowdy, "Exogenous siRNA delivery using peptide transduction domains/cell penetrating peptides," *Adv Drug Deliv Rev,* vol. 59, no. 2-3, pp. 134-40, Mar 30 2007, doi: 10.1016/j.addr.2007.03.004.
[42] A. L. Klibanov *et al.*, "Targeting of macromolecular carriers and liposomes by antibodies to myosin heavy chain," (in eng), *American Journal of Physiology,* vol. 261, no. 0002-9513 (Print), pp. 60-65, 1991.
[43] M. A. Oberli *et al.*, "Lipid Nanoparticle Assisted mRNA Delivery for Potent Cancer Immunotherapy," *Nano Lett,* vol. 17, no. 3, pp. 1326-1335, Mar 8 2017, doi: 10.1021/acs.nanolett.6b03329.

[44] H. Lv, S. Zhang, B. Wang, S. Cui, and J. Yan, "Toxicity of cationic lipids and cationic polymers in gene delivery," *Journal of Controlled Release,* vol. 114, pp. 100-109, April 2006 2006, doi: 10.1016/j.jconrel.2006.04.014.
[45] A. Zubareva, B. Shagdarova, V. Varlamov, E. Kashirina, and E. Svirshchevskaya, "Penetration and toxicity of chitosan and its derivatives," *European Polymer Journal,* vol. 93, pp. 743-749, August 2017 2017, doi: 10.1016/j.eurpolymj.2017.04.021.
[46] A. L. Coolen *et al.*, "Poly(lactic acid) nanoparticles and cell-penetrating peptide potentiate mRNA-based vaccine expression in dendritic cells triggering their activation," *Biomaterials,* vol. 195, pp. 23-37, Mar 2019, doi: 10.1016/j.biomaterials.2018.12.019.
[47] J. U. Menon, P. Ravikumar, A. Pise, D. Gyawali, C. C. Hsia, and K. T. Nguyen, "Polymeric nanoparticles for pulmonary protein and DNA delivery," *Acta Biomaterials,* vol. 10, no. 6, pp. 2643-52, Jun 2014 2014, doi: 10.1016/j.actbio.2014.01.033.
[48] Y. Yan, H. Xiong, X. Zhang, Q. Cheng, and D. J. Siegwart, "Systemic mRNA Delivery to the Lungs by Functional Polyester-based Carriers," *Biomacromolecules,* vol. 18, no. 12, pp. 4307-4315, 2017/12/11 2017, doi: 10.1021/acs.biomac.7b01356.
[49] H. Guerrero-Cázares, S. Y. Tzeng, N. P. Young, A. O. Abutaleb, A. Quiñones-Hinojosa, and J. J. Green, "Biodegradable Polymeric Nanoparticles Show High Efficacy and Specificity at DNA Delivery to Human Glioblastoma in Vitro and in Vivo," *ACS Nano,* vol. 8, no. 5, pp. 5141-5153, 2014/05/27 2014, doi: 10.1021/nn501197v.
[50] E. Inyang, A. Kuriakose, B. Chen, K. Nguyen, and M. Cho, "Engineering Delivery of Nonbiologics Using Poly(lactiv-co-glycolic acid) Nanoparticles for Repair of Disrupted Brain Endothelium," *ACS Omega,* vol. 5, no. 24, pp. 14730-14740, June 2020 2020, doi: 10.1021/acsomega.0c01517.
[51] L. Zangi *et al.*, "Modified mRNA directs the fate of heart progenitor cells and induces vascular regeneration after myocardial infarction," *Nature biotechnology,* vol. 31, no. 10, pp. 898-907, Oct 2013, doi: 10.1038/nbt.2682.
[52] A. Amani, T. Kabiri, S. Shafiee, and A. Hamidi, "Preparation and Characterization of PLA-PEG-PLA/PEI/DNA Nanoparticles for Improvement of Transfection Efficiency and Controlled Release of DNA in Gene Delivery Systems," *Iranian Journal of Pharmaceutical Research,* vol. 18, no. 1, pp. 125-141, April 2018 2019.
[53] N. Ryu *et al.*, "Effective PEI-mediated delivey of CRISPR-Cas9 complex for targeted gene therapy," *Nanomedicine: Nanotechnology, Biology, and Medicine14,* no. 7, pp. 2095-2102, October 2018 2018, doi: 10.1016/j.nano.2018.06.009.
[54] R. C. Cooper and H. Yang, "Duplex of Polyamidoamine Dendrimer/Custom-Designed Nuclear-Localization Sequence Peptide for Enhanced Gene Delivery," *Bioelectrcity,* vol. 2, no. 2, pp. 150-157, June 2020 2020, doi: 10.1089/bioe.2020.0009.
[55] B. Srinageshwar *et al.*, "A Mixed-Surface Polyamidoamine Dendrimer for In Vitro and In Vivo Delivery of Large Plasmids," *Pharmaceutics,* vol. 12, no. 7, p. 619, Jun 2020 2020, doi: 10.3390/pharmaceutics12070619.
[56] T. Huang *et al.*, "Chitosan-DNA nanoparticles enhanced the immunogenicity of multivalent DNA vaccination on mice " *Journal of Nanobiotechnology,* vol. 16, no. 8, January 2018 2018, Art no. 8, doi: 10.1186/s12951-018-0337-2.
[57] S. Rahmani *et al.*, "Novel chitosan based nanoparticles as gene delivery systems to cancerous and noncancerous cells," *International Journal of Pharmaceutics,* vol. 560, pp. 306-314, April 2019 2019, doi: 10.1016/j.ijpharm.2019.02.016.

[58] M. H. Nematollahi, M. Torkzadeh-Mahanai, A. Pardakhty, H. A. E. Meimand, and G. Asadikaram, "Ternary complex of plasmid DNA with NLS-Mu-Mu protein and cationic niosome for biocompatible and efficient gene delivery: A comparative study with protamine and lipofectamine," *Artificial Cells, Nanomedicine, and Biotechnology,* vol. 46, no. 8, pp. 1781-1791, Dec 2017 2017, doi: 10.1080/21691401.2017.1392316 10.1080/21691401.2017.1405231.

[59] E. Marin, M. I. Briceño, and C. Caballero-George, "Critical evaluation of biodegradable polymers used in nanodrugs," *International Journal of Nanomedicine,* vol. 8, pp. 3071-3091, August 2013 2013, doi: 10.2147/IJN.S47186.

[60] J. Patel, J. Amrutiya, P. Bhatt, A. Javia, M. Jain, and A. Misra, "Targeted delivery of monoclonal antibody conjugated docetaxel loaded PLGA nanoparticles into EGFR overexpressed lung tunour cells," *Journal of Microencapsulation,* vol. 35, no. 2, pp. 204-217, March 2018 2018, doi: 10.1080/02652048.2018.1453560.

[61] Y. Malinovskaya *et al.*, "Delivery of doxorubicin-loaded PLGA nanoparticles into U87 human glioblastoma cells," *International Journal of Pharmaceutics,* vol. 524, pp. 77-90, March 2017 2017, doi: 10.1016/j.ijpharm.2017.03.049.

[62] F. Madani, S. S. Esnaashari, B. Mujokoro, F. Dorkoosh, M. Khosravani, and M. Adabi, "Investigation of effective parameters on size of paclitaxel loaded PLGA nanoparticles," *Advanced Pharmaceutical Bulletin,* vol. 8, no. 1, pp. 77-84, February 2018 2018, doi: 10.15171/apb.2018.010.

[63] I. Khan *et al.*, "PLGA Nanoparticles and Their Versatile Role in Anticancer Drug Delivery," vol. 33, no. 2, pp. 159-193, 2016-09-19 2016, doi: 10.1615/CritRevTherDrugCarrierSyst.2016015273.

[64] D. Cun *et al.*, "High Loading efficiency and sustained release of siRNA encapsulated PLGA nanoparticles; Quality by design optimization and characterization," *European Journal of Pharmaceutics and Biopharmaceutics,* vol. 77, no. 1, pp. 26-35, January 2011 2011, doi: 10.1016/j.ejpb.2010.11.008.

[65] J. S. Golub *et al.*, "Sustained VEGF delivery via PLGA nanoparticles promotes vascular growth," *Am J Physiol Heart Circ Physiol,* vol. 298, no. 6, pp. H1959-65, Jun 2010, doi: 10.1152/ajpheart.00199.2009.

[66] Y. Oduk, R. Kannappan, Z. Wuqiang, and J. Zhang, "Abstract 19225: Sustained Release of VEGF via PLGA Nanoparticles Improves Vascularization in vitro and in vivo," *Circulation,* vol. 134, 1, 2016.

[67] S. G. Jeon *et al.*, "Vitamin D-binding protein-loaded PLGA nanoparticles suppress Alzheimer's disease-related pathology in 5XFAD mice," *Nanomedicine: Nanotechnology, Biology, and Medicine14,* vol. 17, pp. 297-307, January 2019 2019, doi: 10.1016/j.nano.2019.02.004.

[68] E. Zhang *et al.*, "Release kinetics of fluorescent dyes from PLGA nanoparticles in retinal blood vessels: In vivo monitoring and ex vivo localization," *European Journal of Pharmaceutics and Biopharmaceutics,* vol. 150, pp. 131-142, March 2020 2020, doi: 10.1016/j.ejpb.2020.03.006.

[69] A. Dalpiaz *et al.*, "Application of the "in-oil nanoprecipitation" method in the encapsulation of hydrophillic drugs in PLGA nanoparticles," *Journal of Drug Delivery Science and Technology,* vol. 32, Part B, pp. 283-290, April 2016 2016, doi: 10.1016/j.jddst.2015.07.020.

[70] A. Dardik *et al.*, "Differential effects of orbital and laminar shear stress on endothelial cells," *J Vasc Surg,* vol. 41, no. 5, pp. 869-80, May 2005, doi: 10.1016/j.jvs.2005.01.020.
[71] W.-J. Cherng, Z.-S. Dong, C.-C. Chou, C.-H. Yeh, and Y.-H. Pan, "Hydrodynamic Simulation of an Orbital Shaking Test for the Degradation Assessment of Blood-Contact Biomedical Coatings," *Micromachines,* vol. 8, no. 4, 2017, doi: 10.3390/mi8040132.
[72] J. Buchs, U. Maier, C. Milbradt, and B. Zoels, "Power Consumption in Shaking Flasks on Rotary Shaking Machines: I. Power Consumption Measurement in Unbaffled Flasks at Low Liquid Viscosity," *Biotechnology Bioengineering,* vol. 68, pp. 589-593, Feb 14 2000.
[73] W. Klockner and J. Buchs, "Advances in shaking technologies," *Trends Biotechnol,* vol. 30, no. 6, pp. 307-14, Jun 2012, doi: 10.1016/j.tibtech.2012.03.001.
[74] G. F. Liang *et al.*, "PLGA-based gene delivering nanoparticle enhance suppression effect of miRNA in HePG2 cells," *Nanoscale Res Lett,* vol. 6, p. 447, Jul 12 2011, doi: 10.1186/1556-276X-6-447.
[75] J. U. Menon *et al.*, "Dual-Drug Containing Core-Shell Nanoparticles for Lung Cancer Therapy," *Scientific Reports,* vol. 7, no. 1, p. 13249, 2017/10/16 2017, doi: 10.1038/s41598-017-13320-4.
[76] P. A. Kalvanagh, M. Ebtekar, P. Kokhaei, and H. Soleimanjahi, "Preparation and Characterization of PLGA Nanoparticles Containng Plasmid DNA Encoding HUman IFN-lambda-1/IL-29," *Iranian Journal of Pharmaceutical Research,* vol. 18, no. 1, pp. 156-167, October 2018 2019.
[77] T. Dastan and K. turan, "In vitro characterization and delivery of chitosan-DNA microparticles into mamalian cells. ," *J Pharm Pharmaceut Sci,* vol. 7, no. 2, pp. 205-214, June 30 2004.
[78] K. Gvili, O. Benny, D. Danino, and M. Machluf, "Poly(D,L-lactide-co-glycolide acid) nanoparticles for DNA delivery: waiving preparation complexity and increasing efficiency," *Biopolymers,* vol. 85, no. 5-6, pp. 379-91, Apr 5-15 2007, doi: 10.1002/bip.20697.
[79] H. K. Makadia and S. J. Siegel, "Poly Lactic-co-Glycolic Acid (PLGA) as Biodegradable Controlled Drug Delivery Carrier," *Polymers (Basel),* vol. 3, no. 3, pp. 1377-1397, Sep 1 2011, doi: 10.3390/polym3031377.
[80] M. Allahyari and E. Mohit, "Peptide/protein vaccine delivery system based on PLGA particles," *Hum Vaccin Immunother,* vol. 12, no. 3, pp. 806-28, Mar 3 2016, doi: 10.1080/21645515.2015.1102804.
[81] C. B. Roces, D. Christensen, and Y. Perrie, "Translating the fabrication of protein-loaded poly(lactic-co-glycolic acid) nanoparticles from bench to scale-independent production using microfluidics," *Drug Deliv Transl Res,* vol. 10, no. 3, pp. 582-593, Jun 2020, doi: 10.1007/s13346-019-00699-y.
[82] M. Haji Mansor *et al.*, "Development of a non-toxic and non-denaturing formulation process for encapsulation of SDF-1alpha into PLGA/PEG-PLGA nanoparticles to achieve sustained release," *Eur J Pharm Biopharm,* vol. 125, pp. 38-50, Apr 2018, doi: 10.1016/j.ejpb.2017.12.020.
[83] Y. Shi, M. Zhou, J. Zhang, and W. Lu, "Preparation and cellular targeting study of VEGF-conjugated PLGA Nanoparticles," *Journal of Microencapsulation,* vol. 32, no. 7, pp. 699-704, 2015, doi: 10.3109/02652048.2015.1035683.

[84] B. Lu, X. Lv, and Y. Le, "Chitosan-Modified PLGA Nanoparticles for Control-Released Drug Delivery," *Polymers (Basel)*, vol. 11, no. 2, Feb 12 2019, doi: 10.3390/polym11020304.
[85] N. Wilkosz *et al.*, "Molecular Insight into Drug-Loading Capacity of PEG-PLGA Nanoparticles for Itraconazole," *J Phys Chem B*, vol. 122, no. 28, pp. 7080-7090, Jul 19 2018, doi: 10.1021/acs.jpcb.8b03742.
[86] X. Yu *et al.*, "Preparation and Characterization of PLGA-PEG-PLGA Nanoparticles Containing Salidroside and Tamoxifen for Breast Cancer Therapy," *AAPS PharmSciTech*, vol. 21, no. 3, p. 85, Jan 29 2020, doi: 10.1208/s12249-019-1523-8.
[87] T. Bettinger, R. C. Carlisle, M. L. Read, M. Ogris, and S. L. W., "Peptide-mediated RNA delivery: a novel approach for enhanced transfection of primary and post-mitotic cells," *Nucleic Acids Res*, vol. 29, no. 18, pp. 3882-3891, 2001, doi: doi.org/10.1093/nar/29.18.3882.
[88] J. Panyam and V. Labhasetwar, "Biodegradable nanoparticles for drug and gene delivery to cells and tissue," *Advanced Drug Delivery Reviews*, vol. 55, no. 3, pp. 329-347, 2003/02/24/ 2003, doi: https://doi.org/10.1016/S0169-409X(02)00228-4.
[89] K. Kamimura, T. Suda, G. Zhang, and D. Liu, "Advances in Gene Delivery Systems," *Pharmaceutical Medicine - New Zealand*, vol. 25, no. 5, pp. 293-306, 2001 2011, doi: 10.1007/BF03256872.
[90] M. H. Oh *et al.*, "Large-scale synthesis of bioinert tantalum oxide nanoparticles for X-ray computed tomography imaging and bimodal image-guided sentinel lymph node mapping," (in eng), *Journal of the American Chemical Society*, vol. 133, no. 14, pp. 5508-5515, 2011, doi: 10.1021/ja200120k.
[91] H. Takahama *et al.*, "Prolonged targeting of ischemic/reperfused myocardium by liposomal adenosine augments cardioprotection in rats," *J Am Coll Cardiol*, vol. 53, no. 8, pp. 709-17, Feb 24 2009, doi: 10.1016/j.jacc.2008.11.014.
[92] I. C. Turnbull *et al.*, "Myocardial Delivery of Lipidoid Nanoparticle Carrying modRNA Induces Rapid and Transient Expression," *MOLECULAR THERAPY*, vol. 24, no. 1, pp. 66-75, 2016, doi: 10.1038/mt.2015.193.
[93] F.-L. Wu *et al.*, "Enhanced antiproliferative activity of antibody-functionalized polymeric nanoparticles for targeted delivery of anti-miR-21 to HER2 positive gastric cancer," *Oncotarget*, vol. 8, no. 40, pp. 67189–67202, 2017, doi: 10.18632/oncotarget.18066.
[94] N. Kumskova *et al.*, "How subtle differences in polymer molecular weight affect doxorubicin-loaded PLGA nanoparticles degradation and drug release," *J Microencapsul*, vol. 37, no. 3, pp. 283-295, May 2020, doi: 10.1080/02652048.2020.1729885.
[95] Y. Choi *et al.*, "Doxorubicin-Loaded PLGA Nanoparticles for Cancer Therapy: Molecular Weight Effect of PLGA in Doxorubicin Release for Controlling Immunogenic Cell Death," *Pharmaceutics*, vol. 12, no. 12, Nov 29 2020, doi: 10.3390/pharmaceutics12121165.
[96] G. Mittal, D. K. Sahana, V. Bhardwaj, and M. N. Ravi Kumar, "Estradiol loaded PLGA nanoparticles for oral administration: effect of polymer molecular weight and copolymer composition on release behavior in vitro and in vivo," *J Control Release*, vol. 119, no. 1, pp. 77-85, May 14 2007, doi: 10.1016/j.jconrel.2007.01.016.
[97] A. A. Ozturk, E. Yenilmez, B. Senel, H. T. Kiyan, and U. M. Guven, "Effect of different molecular weight PLGA on flurbiprofen nanoparticles: formulation, characterization,

cytotoxicity, and in vivo anti-inflammatory effect by using HET-CAM assay," *Drug Dev Ind Pharm*, vol. 46, no. 4, pp. 682-695, Apr 2020, doi: 10.1080/03639045.2020.1755304.
[98] Y. M. Thasneem, S. Sajeesh, and C. P. Sharma, "Effect of thiol functionalization on the hemo-compatibility of PLGA nanoparticles," *J Biomed Mater Res A*, vol. 99, no. 4, pp. 607-17, Dec 15 2011, doi: 10.1002/jbm.a.33220.
[99] J. Zhang *et al.*, "Protein-Polymer Nanoparticles for Novel Gene Delivery," *Biomacromolecules*, vol. 12, no. 4, pp. 1006–1014, Feb 16, 2011 2011, doi: 10.1021/bm101354a.
[100] J. Chen, K. Wang, J. Wu, H. Tian, and X. Chen, "Polycations for Gene Delivery: Dilemmas and Solutions," *Bioconjug Chem*, vol. 30, no. 2, pp. 338-349, Feb 20 2019, doi: 10.1021/acs.bioconjchem.8b00688.
[101] N. Amreddy, A. Babu, R. Muralidharan, A. Munshi, and R. Ramesh, "Polymeric Nanoparticle-Mediated Gene Delivery for Lung Cancer Treatment," *Top Curr Chem (Cham)*, vol. 375, no. 2, p. 35, Apr 2017, doi: 10.1007/s41061-017-0128-5.
[102] M. Uhlén *et al.*, "Tissue-based map of the human proteome," *Science*, vol. 347, no. 6220, p. 1260419, 2015, doi: 10.1126/science.1260419.
[103] P. Kocbek, N. Obermajer, M. Cegnar, J. Kos, and J. Kristl, "Targeting cancer cells using PLGA nanoparticles surface modified with monoclonal antibody," *J Control Release*, vol. 120, no. 1-2, pp. 18-26, Jul 16 2007, doi: 10.1016/j.jconrel.2007.03.012.
[104] J. Duan, Y. Yu, Y. Li, Y. Yu, and Z. Sun, "Cardiovascular toxicity evaluation of silica nanoparticles in endothelial
cells and zebrafish model," *Biomaterials*, vol. 34, no. 23, pp. 5853-5862, 2013, doi: 10.1016/j.biomaterials.2013.04.032.
[105] A. C. Anselmo and S. Mitragotri, "Nanoparticles in the clinic," *Bioeng Transl Med*, vol. 1, no. 1, pp. 10-29, Mar 2016, doi: 10.1002/btm2.10003.
[106] A. L. Cortajarena *et al.*, "Engineering Iron Oxide Nanoparticles for Clinical Settings," *Nanobiomedicine (Rij)*, vol. 1, p. 2, Jan-Dec 2014, doi: 10.5772/58841.
[107] Y. Min, J. M. Caster, M. J. Eblan, and A. Z. Wang, "Clinical Translation of Nanomedicine," *Chem Rev*, vol. 115, no. 19, pp. 11147-90, Oct 14 2015, doi: 10.1021/acs.chemrev.5b00116.
[108] S. Hua, "Lipid-based nano-delivery systems for skin delivery of drugs and bioactives," *Front Pharmacol*, vol. 6, p. 219, 2015, doi: 10.3389/fphar.2015.00219.
[109] Y. Barenholz, "Doxil(R)--the first FDA-approved nano-drug: lessons learned," *J Control Release*, vol. 160, no. 2, pp. 117-34, Jun 10 2012, doi: 10.1016/j.jconrel.2012.03.020.
[110] J. Bakkers, "Zebrafish as a model to study cardiac development and human cardiac disease," *Cardiovascular Research*, vol. 91, no. 2, pp. 279-288, 05/19
01/18/received
03/22/revised
04/01/accepted 2011, doi: 10.1093/cvr/cvr098.
[111] S. Isogai, M. Horiguchi, and B. M. Weinstein, "The Vascular Anatomy of the Developing Zebrafish: An Atlas of Embryonic and Early Larval Development," *Developmental Biology*, vol. 230, no. 2, pp. 278-301, 2001, doi: 10.1006/dbio.2000.9995.
[112] D. J. Milan, I. L. Jones, P. T. Ellinor, and C. A. MacRae, "In vivo recording of adult zebrafish electrocardiogram and assessment of drug-induced QT prolongation," *Am J Physiol Heart Circ Physiol*, vol. 291, no. 1, pp. H269-73, Jul 2006, doi: 10.1152/ajpheart.00960.2005.

[113] D. Sedmera *et al.*, "Functional and morphological evidence for a ventricular conduction system in zebrafish and Xenopus hearts," *Am J Physiol Heart Circ Physiol,* vol. 284, no. 4, pp. H1152-H1160, 01 April 2003, doi: doi.org/10.1152/ajpheart.00870.2002.
[114] J. Lee *et al.*, "Hemodynamics and Ventricular Function in a Zebrafish Model of Injury and Repair," *Zebrafish,* vol. 11, no. 5, pp. 447-454, 2014, doi: 10.1089/zeb.2014.1016.
[115] C. M. Hull *et al.*, "Investigating the utility of adult zebrafish ex vivo whole hearts to pharmacologically screen hERG channel activator compounds," *Am J Physiol Regul Integr Comp Physiol,* vol. 317, no. 6, pp. R921-R931, Dec 1 2019, doi: 10.1152/ajpregu.00190.2019.
[116] N. Milani-Nejad and P. M. Janssen, "Small and large animal models in cardiac contraction research: advantages and disadvantages," *Pharmacol Ther,* vol. 141, no. 3, pp. 235-49, Mar 2014, doi: 10.1016/j.pharmthera.2013.10.007.
[117] K. A. Smith *et al.*, "Dominant-negative ALK2 allele associates with congenital heart defects," *Circulation,* vol. 119, no. 24, pp. 3062-9, Jun 23 2009, doi: 10.1161/CIRCULATIONAHA.108.843714.
[118] A. J. Hill, H. Teraoka, W. Heideman, and R. E. Peterson, "Zebrafish as a model vertebrate for investigating chemical toxicity," *Toxicol Sci,* vol. 86, no. 1, pp. 6-19, Jul 2005, doi: 10.1093/toxsci/kfi110.
[119] Y.-L. Hu, W. Qi, F. Han, J.-Z. Shao, and J.-Q. Gao, "Toxicity evaluation of biodegradable chitosan
nanoparticles using a zebrafish embryo model," *International Journal of Nanomedicine,* vol. 6, pp. 3351–3359, 2011, doi: 10.2147/IJN.S25853.
[120] C. Teijeiro-Valiño, E. Yebra-Pimentel, J. Guerra Varela, N. Csaba, M. J. Alonso, and L. Sánchez, "Assessment of the permeability and toxicity of polymeric nanocapsules using the zebrafish model," *NanoMedicine,* vol. 12, no. 17, 2017, doi: https://doi.org/10.2217/nnm-2017-0078.
[121] H. C. Yalcin, A. Amindari, J. T. Butcher, A. Althani, and M. Yacoub, "Heart function and hemodynamic analysis for zebrafish embryos," *Dev Dyn,* vol. 246, no. 11, pp. 868-880, Nov 2017, doi: 10.1002/dvdy.24497.
[122] K. A. Kurnia *et al.*, "Measurement of Multiple Cardiac Performance Endpoints in Daphnia and Zebrafish by Kymograph," *Inventions,* vol. 6, no. 1, 2021, doi: 10.3390/inventions6010008.
[123] S. N. Dash *et al.*, "Sept7b is required for the subcellular organization of cardiomyocytes and cardiac function in zebrafish," *Am J Physiol Heart Circ Physiol,* vol. 312, no. 5, pp. H1085-H1095, May 1 2017, doi: 10.1152/ajpheart.00394.2016.
[124] H. C. Tu *et al.*, "One crisis, diverse impacts-Tissue-specificity of folate deficiency-induced circulation defects in zebrafish larvae," *PLoS One,* vol. 12, no. 11, p. e0188585, 2017, doi: 10.1371/journal.pone.0188585.